Nationaal Lucht- en Ruimtevaartlaboratorium

National Aerospace Laboratory NLR

NLR-TP-2013-294

Low-Order Modeling For A Small-Scale Flybarless Helicopter UAV

A Grey-Box Time-Domain Approach

S. Taamallah

Nationaal Lucht- en Ruimtevaartlaboratorium
National Aerospace Laboratory NLR

Anthony Fokkerweg 2
P.O. Box 90502
1006 BM Amsterdam
The Netherlands
Telephone +31 (0)88 511 31 13
Fax +31 (0)88 511 32 10
www.nlr.nl

Nationaal Lucht- en Ruimtevaartlaboratorium

National Aerospace Laboratory NLR

Executive summary

Low-Order Modeling For A Small-Scale Flybarless Helicopter UAV

A Grey-Box Time-Domain Approach

Problem area
We present a flight dynamics nonlinear model for a flybarless helicopter UAV, valid for a range of flight conditions, including the Vortex-Ring-State (VRS) and autorotation.

Description of work
The model includes the main rotor, tail rotor, fuselage, and tails. To allow for computational efficiency, while maintaining a high-level of model fidelity, a combined grey-box multiple-model approach has been adopted, in which model uncertainty such as unmodeled higher-order dynamics and unmodeled static nonlinearities have been replaced by empirical coefficients. These coefficients have been identified, through parameter estimation techniques, from FLIGHTLAB data. Additionally, the paper reviews all assumptions made in deriving the model, i.e. structural, aerodynamics, and dynamical simplifications.

Results and conclusions
Preliminary simulation results show that the fit between this model and an equivalent nonlinear FLIGHTLAB model is good to very good, both for static and dynamic flight conditions.

Applicability
Development of flight control systems for small-scale UAV helicopters.

Report no.
NLR-TP-2013-294

Author(s)
S. Taamallah

Report classification
UNCLASSIFIED

Date
June 2014

Knowledge area(s)
Helikoptertechnologie

Descriptor(s)
Unmanned Aerial Vehicle (UAV)
Helicopter Flight Dynamics

This report is based on a presentation held at the AIAA Atmospheric Flight Mechanics Conference August 13 – 16, 2012, Minneapolis, Minnesota.

Nationaal Lucht- en Ruimtevaartlaboratorium, National Aerospace Laboratory NLR

Anthony Fokkerweg 2, 1059 CM Amsterdam,
P.O. Box 90502, 1006 BM Amsterdam, The Netherlands
Telephone +31 88 511 31 13, Fax +31 88 511 32 10, Web site: www.nlr.nl

Nationaal Lucht- en Ruimtevaartlaboratorium

National Aerospace Laboratory NLR

NLR-TP-2013-294

Low-Order Modeling For A Small-Scale Flybarless Helicopter UAV

A Grey-Box Time-Domain Approach

S. Taamallah

This report is based on a presentation held at the AIAA Atmospheric Flight Mechanics Conference August 13 – 16, 2012, Minneapolis, Minnesota.

The contents of this report may be cited on condition that full credit is given to NLR and the authors.

Customer	National Aerospace Laboratory NLR
Contract number	----
Owner	NLR
Division NLR	Aerospace Systems and Applications
Distribution	Unlimited
Classification of title	Unclassified
	June 2014

Approved by:

Author	Reviewer	Managing department
Date: 1/11/2013	Date: 1/11/2013	Date: 15/11/2013

Contents

I.	Introduction	5
I.A.	The Modeling Framework In Engineering	6
I.B.	Helicopter UAV Modeling Background	6
I.C.	Our Grey-Box Helicopter Model	7
II.	Rigid Body Equations of Motion	7
II.A.	Assumptions	7
II.B.	Modeling	8
III.	Main Rotor Modeling	9
III.A.	Assumptions	9
II.B.	ModeliIng	10
IV.	Tail Rotor Modeling	15
IV.A.	Assumptions	15
IV.B.	Modeling	15
V.	Fuselage Modeling	17
V.A.	Assumptions	17
VI.	Vertical Tail Modeling	19
VI.	Vertical Tail Modeling	19

VI.B.	Modeling	19
VII.	Horizontal Tail Modeling	20
VII.A.	Assumptions	20
VII.B.	Modeling	20
VIII.	Black-Box Modeling	22
VIII.A.	The Multiple-Model Approach	22
VIII.B.	Black-Box: Modeling Framework	22
VIII.C.	Improving The Static White-Box Behavior	23
VIII.D.	Improving The Dynamic White-Box Behavior	24
VIII.E.	Validation	28
IX.	Simulation Results	28
IX.A.	Trim Results	29
IX.B.	Dynamic Results	29
X.	Conclusion	30
Appendix A: Nomenclature		31
Appendix B: Physical Parameters		38
Appendix C: Simulation Results		39
References		44

Low-Order Modeling For A Small-Scale Flybarless Helicopter UAV A Grey-Box Time-Domain Approach

Skander Taamallah*†

National Aerospace Laboratory (NLR), 1059CM Amsterdam, The Netherlands

We present a flight dynamics nonlinear model for a flybarless helicopter UAV, valid for a range of flight conditions, including the Vortex-Ring-State (VRS) and autorotation. The model includes the main rotor, tail rotor, fuselage, and tails. To allow for computational efficiency, while maintaining a high-level of model fidelity, a combined grey-box multiple-model approach has been adopted, in which model uncertainty such as unmodeled higher-order dynamics and unmodeled static nonlinearities have been replaced by empirical coefficients. These coefficients have been identified, through parameter estimation techniques, from FLIGHTLAB® data. Additionally, the paper reviews all assumptions made in deriving the model, i.e. structural, aerodynamics, and dynamical simplifications. Preliminary simulation results show that the fit between this model and an equivalent nonlinear FLIGHTLAB model is good to very good, both for static and dynamic flight conditions.

Nomenclature

The nomenclature is given in Appendix A.

I. Introduction

In the past twenty years, scientific progress related to sensors technology and computational hardware has allowed for sustained research in the field of robotics. In particular, when considering flying robots, the availability of increasingly reliable, high performance, and miniaturized sensors, combined with advances in computing power on miniaturized hardware, has yielded impressive developments in the area of Unmanned Aerial Vehicles (UAVs)[a]. These unmanned vehicles have been developed for both civilian and military missions[b], while their *raison d'être* stems from the need for (real-time) information[c]. Further, UAV deployment and recovery from unprepared or confined sites may often be necessary, such as when operating from or above urban and natural canyons, forests, or naval ships. Hence, for these situations, a helicopter UAV capable of flying in and out of such restricted areas would represent a particularly attractive solution. Now, the development of such an autonomous helicopter system requires for an elaborate synergy between various engineering fields, including modeling, system identification, estimation and filtering, control, and finally software and hardware avionics integration. In this paper, we elaborate on the first item, i.e. the modeling paradigm.

*R&D Engineer, Aircraft Systems Department, National Aerospace Laboratory (NLR), 1059CM Amsterdam, The Netherlands.

†Ph.D. Student, Delft Center for Systems and Control (DCSC), Faculty of Mechanical, Maritime and Materials Engineering, Delft University of Technology, 2628CD Delft, The Netherlands.

[a]Although industry and the regulators have now adopted Unmanned Aerial System (UAS) as the preferred term for Unmanned Aircraft, as UAS encompasses all aspects of deploying these vehicles and not just the platform itself.

[b]UAVs have typically been associated with the so-called *DDD* tasks:[1] Dull e.g. long duration, Dirty e.g. sampling for hazardous materials, and Dangerous e.g. extreme exposure to hostile action.

[c]Spanning a broad spectrum, i.e. visual, electromagnetic, physical, nuclear, biological, chemical, or meteorological information.

I.A. The Modeling Framework In Engineering

There are two fundamentally different philosophies that form the basis of modeling, namely the so-called mechanistic (or first-principles) one, and the empirical one.[2] In the first case, a white-box model structure is developed on the basis of detailed understandings of the generic underlying physical laws, that govern the system, while in the second case a black-box model is derived on the basis of specific observed system behaviors. Overall, the first-principles based models substantially contribute to a scientific understanding of its comportment, while the empirical based models allow for simpler representations, and quicker design and development cycles, as a deeper understanding of the system's laws is neither always required, nor necessary.[2]

Both of these approaches, when used independently, may often be unattractive. If the system's first-principles laws may only be partially understood, the development of a white-box model may end up being very challenging, at best, while delivering an end-product with questionable model fidelity. In some complex industrial cases, even when the laws of physics may be well comprehended, the development and validation of such white-box models may turn out to be highly resource demanding. Additionally, the intended model application may as well impose restrictions on its structure and complexity. Indeed, depicting a system with an accurate mathematical representation, in a computationally tractable way for its intended application, may result in conflicting requirements.[3] On the other hand, the development of a black-box model may be impaired by the well-known principle of induction[d] deficiencies. Indeed, it is widely accepted that induction has serious limitations, as a finite number of observations is generally not sufficient to envelop the infinite number of model operating regimes[e].[2,4]

Hence, for practical applications, many models are based on a mixing of mechanistic and empirical knowledge, resulting in a grey-box model, also known as the hybrid modeling paradigm.[5] For instance, in a mainly white-box approach, aspects of the system that are not sufficiently well understood, which in general are regrouped under the umbrella of model uncertainties (i.e. unmodeled higher-order dynamics, unmodeled static nonlinearities, parametric uncertainties, and delays) may be described by an empirical model, this latter being identified through parameter estimation techniques based upon experimental data. Alternatively, in a predominantly black-box approach, some physical understanding may often be useful to make certain structural choices, such as the adequate model order and the nature of its nonlinearities.[2] Consequently, grey-box models, with the necessary help of some engineering skills, combine cheaper development costs, with the required end-product accuracy and reliability, while allowing for computational tractability. By so doing, hybrid models have attracted a growing share of attention, with the increasing demand for nonlinear models to be applied in intelligent and autonomous vehicles, diagnosis systems, and optimization based disciplines.

With this in mind, and since the intended model application is optimal trajectories computation through nonlinear constrained optimal control,[6,7] we opted for a modeling framework, i.e. a grey-box representation, that supports the development of computationally efficient, yet accurate nonlinear dynamic models, valid under a wide range of operating conditions.

I.B. Helicopter UAV Modeling Background

A helicopter is a complex system, and understanding helicopter flight has been a continuous endeavor. Certainly helicopter nonlinear flight dynamics modeling has seen extensive development over the past forty years. Now, in the realm of small-scale helicopter UAV, the past fifteen to twenty years have seen considerable worldwide activity in research[f] related to automatic flight of small-scale helicopter UAVs. For example, for low to medium-bandwidth systems, the usual robustness-performance trade-off has undeniably allowed for quick and successful demonstration (or simulation) of automatic helicopter flight for hover and low speed conditions, see Ref. 8–18. Further, for high-bandwidth system specifications, at still conventional flight con-

[d] The principle of induction suggests that it is possible to generalize from a sufficiently large number of consistent observations.[2,4]

[e] The region for which the model is locally valid is called an operating regime.

[f] In the sequel, due to time and space constraints, we only review contributions in the field of helicopter UAV modeling for control synthesis, excluding thus system identification, navigation, and control aspects.

ditions, model-based automatic flight results can be found in Ref. 19–32, and non-model[g]-based examples have been documented in Ref. 33–36, while vision based systems have been reported in Ref. 37–42. Finally, for high-bandwidth system specifications for aerobatic flight conditions, model-based automatic flight results can be found in Ref. 43–45, whereas non-model-based approaches are given in Ref. 46–48.

In Ref. 49–51, we also presented a high-bandwidth helicopter model, hence including main rotor high-order dynamics, and valid for unconventional flight conditions, such as the Vortex-Ring-State (VRS) and autorotation. Such a model is particularly well suited for high-fidelity simulations, and for the design of high-bandwidth control systems. However, for the case of optimal flight trajectories generation in a computational acceptable way, we needed to rely upon the grey-box modeling paradigm.

I.C. Our Grey-Box Helicopter Model

The purpose of this paper is to present such a model, i.e. a computationally efficient, low-order, yet grey-box flight dynamics model, for the case of a small-scale flybarless[h] helicopter UAV, and valid for a range of flight conditions including the Vortex-Ring-State (VRS) and autorotation. Our nonlinear dynamic white-box model includes the twelve-states rigid body equations of motion, the single-state main rotor Revolutions Per Minute (RPM), a static Tip-Path-Plane (TPP) main rotor model, and a static uniform main rotor inflow model. Besides, the model accommodates for flight in the VRS, and for deterministic wind and Dryden stochastic atmospheric turbulence. Further, static ground effect has been accounted for by a correction factor applied to the non-dimensional total velocity at the rotor disk center. The fuselage model is based upon aerodynamic lift and drag coefficients, which are tabulated as a function of airflow angle of attack and sideslip angles. These lookup tables are derived from a scaled-down full-size helicopter fuselage aerodynamic model. The horizontal and vertical tails are based upon flat plate models, whereas the tail rotor has been modeled as a Bailey type rotor. Finally the paper reviews all assumptions made in deriving the model, i.e. structural, aerodynamics, and dynamical simplifications, which are valid for stability and control investigations of helicopters up to an advance ratio limit[i] of about 0.3.[52–54]

The remainder of the paper is organized as follows. In Section II, the rigid body equations of motion are summarized. In Section III, the main rotor model is discussed. In Section IV, the tail rotor model is presented. In Section V, the fuselage model is reviewed. In Sections VI and VII, the vertical and horizontal tail models are outlined. In Section VIII, the black-model framework together with the identification of the empirical coefficients are presented. In Section IX, simulation results are analyzed. Finally, conclusions and future directions are presented in Section X.

II. Rigid Body Equations of Motion

II.A. Assumptions

- The vehicle has a longitudinal plane of symmetry, and has constant mass, inertia, and Center of Gravity (CG) position, hence fuel consumption and/or payload pickup/release are neglected. The vehicle is also a rigid system, i.e. it does not contain any flexible structures, hence the time derivative of the inertia matrix is zero. Further variations of helicopter CG locations due to main rotor blades position are neglected.
- The vehicle height above ground is very small compared to the earth radius, implying a gravitation independent of height and thus constant. Additionally the center of mass and CG are identical for a constant gravity field.
- The earth is assumed fixed and flat. There is then no longer a distinction between the directions of gravitational force and the force of gravity, hence the external force becomes the force of gravity[j].

[g] We refer here to models which are generally not derived from first principles, such as in the areas of machine learning, evolutionary, and genetic algorithms.
[h] Without a Bell-Hiller stabilizing bar.
[i] The flight envelope of small-scale helicopters is well within this limit.
[j] For further details on the geoid earth and gravity see Ref. 55, 56.

Gravity is also a function of latitude, for all practical purpose we will consider the medium latitudes of 52°.

- Finally, we neglect the effect of buoyancy or Armichedes force, which is negligible with respect to all other forces.

II.B. Modeling

To start, our model is defined by a thirteen-state vector, and a four-control input vector

$$\begin{aligned} \mathbf{x} &= \begin{pmatrix} x_N & x_E & x_Z & \phi & \theta & \psi & u & v & w & p & q & r & \Omega_{MR} \end{pmatrix}^T \\ \mathbf{u} &= \begin{pmatrix} \theta_0 & \theta_{TR} & \theta_{1c} & \theta_{1s} \end{pmatrix}^T \end{aligned} \tag{1}$$

Then, classical Newtonian mechanics and the fundamental relationship of kinematics provide us with the standard twelve-state rigid body equations of motion, following notations of Ref. 55.

$$\begin{pmatrix} \dot{x}_N \\ \dot{x}_E \\ \dot{x}_Z \end{pmatrix}^o = \begin{pmatrix} V_N \\ V_E \\ V_Z \end{pmatrix}^o \qquad \begin{pmatrix} V_N \\ V_E \\ V_Z \end{pmatrix}^o = \mathbb{T}_{ob}. \begin{pmatrix} u \\ v \\ w \end{pmatrix}^b \tag{2}$$

$$\begin{pmatrix} \dot{u} \\ \dot{v} \\ \dot{w} \end{pmatrix}^b = - \begin{pmatrix} q.w - r.v \\ r.u - p.w \\ p.v - q.u \end{pmatrix}^b + g. \begin{pmatrix} -\sin\theta \\ \cos\theta\sin\phi \\ \cos\theta\cos\phi \end{pmatrix}^b + \frac{\mathbf{F}_{aero,G_{Fus}}}{m_{Fus}}^b \tag{3}$$

$$\begin{pmatrix} \dot{p} \\ \dot{q} \\ \dot{r} \end{pmatrix}^b = \mathbb{I}_{Fus}^{-1}. \left[\mathbf{M}^b_{G_{Fus}} - \begin{pmatrix} p \\ q \\ r \end{pmatrix}^b \times \left[\mathbb{I}_{Fus}. \begin{pmatrix} p \\ q \\ r \end{pmatrix}^b \right] \right] \tag{4}$$

$$\begin{pmatrix} \dot{\phi} \\ \dot{\theta} \\ \dot{\psi} \end{pmatrix}^b = \begin{pmatrix} 1 & \sin\theta.\frac{\sin\phi}{\cos\theta} & \sin\theta.\frac{\cos\phi}{\cos\theta} \\ 0 & \cos\phi & -\sin\phi \\ 0 & \frac{\sin\phi}{\cos\theta} & \frac{\cos\phi}{\cos\theta} \end{pmatrix} . \begin{pmatrix} p \\ q \\ r \end{pmatrix}^b \tag{5}$$

$$\mathbb{T}_{ob} = \begin{pmatrix} \cos\theta\cos\psi & \sin\theta\sin\phi\cos\psi - \sin\psi\cos\phi & \cos\psi\sin\theta\cos\phi + \sin\phi\sin\psi \\ \sin\psi\cos\theta & \sin\theta\sin\phi\sin\psi + \cos\psi\cos\phi & \sin\theta\cos\phi\sin\psi - \sin\phi\cos\psi \\ -\sin\theta & \cos\theta\sin\phi & \cos\theta\cos\phi \end{pmatrix} \tag{6}$$

With $\mathbf{F}^b_{aero,G_{Fus}}$ the aerodynamic forces experienced by the fuselage CG in the body frame F_b, and $\mathbf{M}^b_{G_{Fus}}$ the moments of all forces expressed at the fuselage[k] CG in frame F_b.

These total forces include contributions from the main rotor, tail rotor, fuselage, vertical tail, and horizontal tail, and are given by

$$\mathbf{F}^b_{aero,G_{Fus}} = \begin{pmatrix} F_{Xaero,G_{Fus}} \\ F_{Yaero,G_{Fus}} \\ F_{Zaero,G_{Fus}} \end{pmatrix}^b = \begin{pmatrix} F_{x_{MR}} \\ F_{y_{MR}} \\ F_{z_{MR}} \end{pmatrix}^b + \begin{pmatrix} F_{x_{TR}} \\ F_{y_{TR}} \\ F_{z_{TR}} \end{pmatrix}^b + \begin{pmatrix} F_{x_F} \\ F_{y_F} \\ F_{z_F} \end{pmatrix}^b + \begin{pmatrix} F_{x_{VT}} \\ F_{y_{VT}} \\ F_{z_{VT}} \end{pmatrix}^b + \begin{pmatrix} F_{x_{HT}} \\ F_{y_{HT}} \\ F_{z_{HT}} \end{pmatrix}^b \tag{7}$$

[k]Note that fuselage inertia and fuselage CG are used here rather than vehicle inertia and vehicle CG, since in the moments term $\mathbf{M}^b_{G_{Fus}}$ we have already accounted for rotor moments due to main rotor inertial loads.

And the total moments, which also include the components due to the non-collocation of the vehicle CG and fuselage CG, are given by

$$\mathbf{M}^b_{aero,G_{Fus}} = \begin{pmatrix} M_{x_{MR}} \\ M_{y_{MR}} \\ M_{z_{MR}} \end{pmatrix}^b + \begin{pmatrix} M_{x_{TR}} \\ M_{y_{TR}} \\ M_{z_{TR}} \end{pmatrix}^b + \begin{pmatrix} M_{x_F} \\ M_{y_F} \\ M_{z_F} \end{pmatrix}^b + \begin{pmatrix} M_{x_{VT}} \\ M_{y_{VT}} \\ M_{z_{VT}} \end{pmatrix}^b + \begin{pmatrix} M_{x_{HT}} \\ M_{y_{HT}} \\ M_{z_{HT}} \end{pmatrix}^b + \begin{pmatrix} -y_F.F_{Zaero,G_{Fus}} + z_F.F_{Yaero,G_{Fus}} \\ -z_F.F_{Xaero,G_{Fus}} + x_F.F_{Zaero,G_{Fus}} \\ -x_F.F_{Yaero,G_{Fus}} + y_F.F_{Xaero,G_{Fus}} \end{pmatrix}^b \quad (8)$$

The derivation of these forces and moments is given in the next sections.

III. Main Rotor Modeling

III.A. Assumptions

Structural Simplifications

- Rotor shaft forward and lateral tilt-angles are zero. The blade has zero twist, constant chord, zero sweep, constant thickness ratio, and a uniform mass distribution.
- Rigid rotor blade in bending. Neglecting higher modes (harmonics), since higher modes are only pronounced at high speed.[57,58] Further, blade torsion is neglected since small-scale helicopter blades are generally relatively stiff.
- Rotor inertia inboard of the flap hinge is assumed small and thus neglected.

Aerodynamics Simplifications

- Vehicle flies at a low altitude, hence neglecting air density and temperature variations. Blade element theory[l] is used to compute rotor lift and drag forces. Radial flow along blade span is ignored. Pitch, lag, and flap angles are assumed to be small.
- Momentum theory[m] is used to compute the uniform inflow component.
- Compressibility effects are disregarded, which is a reasonable assumption considering small-scale helicopter flight characteristics. Viscous flow effects are also disregarded, which is a valid assumption for low angle of attacks and un-separated flow.[61,62]
- Aerodynamic interference effects between the main rotor and other helicopter modules, e.g. fuselage or tail rotor, are neglected.
- When deriving an expression for the main rotor torque (i.e. yaw moment), only a vertical flight inflow and power component is considered, hence omitting forward flight contributions.
- The presence of the fuselage just under the main rotor acts as a so-called pseudo-ground effect, resulting in some thrust recovery. This phenomenon is neglected in our paper, although an estimate of its effect may be obtained from Ref. 63.

Dynamical Simplifications

[l] Calculates the forces on the blade due to its motion through the air. It is assumed that each blade section acts as a 2-D airfoil to produce aerodynamic forces, with the influence of the wake contained in an induced angle of attack at the blade section.[59]

[m] States that the total force acting on a control volume is equal to the rate of change of momentum, i.e. mass flow entering and leaving this control volume.[59,60]

- Dynamic twist[n] is neglected. Hence blade CG is assumed to be located on the blade section quarter chord line.
- Unsteady (frequency dependent) effect for time-dependent development of blade lift and pitching moment, due to changes in local incidence are ignored. For example dynamic stall, due to rapid pitch changes, is ignored.
- A balanced rotor is assumed. In general most of the inertial terms, contributing to main rotor moments, vanish[o] when integrated around 2π azimuth.

III.B. Modeling

III.B.1. Velocities

The main rotor hub aerodynamic velocity in the body frame F_b is given by

$$\mathbf{V}^b_{a,MR} = \begin{pmatrix} V_{a,MR_u} \\ V_{a,MR_v} \\ V_{a,MR_w} \end{pmatrix}^b = \begin{pmatrix} u + (q - q_w).z_H - (r - r_w).y_H \\ v - (p - p_w).z_H + (r - r_w).x_H \\ w + (p - p_w).y_H - (q - q_w).x_H \end{pmatrix}^b - \begin{pmatrix} u_w \\ v_w \\ w_w \end{pmatrix}^b \tag{9}$$

With

$$\begin{pmatrix} u_w \\ v_w \\ w_w \end{pmatrix}^b = \mathbb{T}_{bo}.\begin{pmatrix} u_w \\ v_w \\ w_w \end{pmatrix}^o \quad \text{and} \quad \mathbb{T}_{bo} = \mathbb{T}_{ob}^{-1} \tag{10}$$

And the non-dimensional velocities are expressed as follows

$$\mu_x = -V_{a,MR_u}/V_{MRref} \tag{11a}$$
$$\mu_y = -V_{a,MR_v}/V_{MRref} \tag{11b}$$
$$\mu_z = -V_{a,MR_w}/V_{MRref} \tag{11c}$$
$$\mu_{xy} = \sqrt{\mu_x^2 + \mu_y^2} \quad \text{and} \quad V_{MRref} = \Omega_{MR}.R_{rot} \tag{11d}$$

III.B.2. Inflow

As for the inflow, we consider only the uniform component and we neglect inflow dynamics. Our model is a simplified implementation of the expressions presented in Ref. 65, 66, with the inclusion of the VRS correction from Ref. 67. The momentum theory induced flow λ_m is given from Ref. 59

$$\lambda_m^2.\Big[(\lambda_m + \mu_z)^2 + \mu_{xy}^2\Big] = \left(\frac{v_h}{V_{MRref}}\right)^4 \quad \text{if} \quad \mu_z \geq 0 \quad \text{or} \quad \mu_z.\frac{V_{MRref}}{v_h} \leq -2 \tag{12}$$

In the VRS, it is given from Ref. 67

$$\lambda_m^2.\Big[(\lambda_m + \mu_z)^2 + \mu_{xy}^2 + \left(\frac{v_h}{V_{MRref}}\right)^2.f(\bar{\mu_{xy}}).g(\bar{\lambda})\Big] = \left(\frac{v_h}{V_{MRref}}\right)^4 \quad \text{if} \quad \mu_z.\frac{V_{MRref}}{v_h} \in [-2, 0] \tag{13}$$

[n] Any offset in blade chordwise CG or aerodynamic center position will result in a coupling of the flap and torsion Degrees Of Freedom (DOF) in blade elastic modes.[57]

[o] These terms should be retained when evaluating rotor out-of-balance loads.[64]

In the static case, also from Ref. 65, 66, the rotor uniform induced velocity, normal to the TPP, is given by

$$v_{i_o} = G_{eff}/(2V_T).(-C_T^{TPP}).V_{MRref} \tag{14}$$

Where C_T^{TPP} is the main rotor thrust coefficient in the TPP frame. Since the TPP angles are assumed small, we conjecture that it is also valid in the Hub-Body frame, i.e. $C_T^{HB} \simeq C_T^{TPP}$. Now, from Ref. 59 we get, after rearranging terms, the thrust coefficient in the Hub-Body frame

$$\begin{aligned} C_T^{HB} &= A + B.v_{i_o} \quad \text{with} \\ A &= -0.5.\sigma_{MR}.CL_{MR_\alpha}.\theta_0/3.(B^3 + 1.5B.\mu_{xy}^2) \\ &\quad -0.25.\sigma_{MR}.CL_{MR_\alpha}.B^2.\Big(V_{a,MR_w}/V_{MRref} + \mu_{xy}.(\beta_{1c} + \theta_{1s})\Big) \\ B &= 0.25.\sigma_{MR}.CL_{MR_\alpha}.B^2/V_{MRref} \end{aligned} \tag{15}$$

And V_T gives the total flow,[67] through the rotor disk, as

$$V_T = \Theta_{MRvrs}.\sqrt{(\lambda_m + \mu_z)^2 + \mu_{xy}^2 + (v_h/V_{MRref})^2.f(\bar{\mu_{xy}}).g(\bar{\lambda})} \tag{16}$$

With the following correction factors

$$\begin{aligned} f(\bar{\mu_{xy}}) &= 1 - 2.\bar{\mu_{xy}}^2 \quad \text{if} \quad \bar{\mu_{xy}} \in [0, 0.707] \\ f(\bar{\mu_{xy}}) &= 0 \quad \text{otherwise} \\ g(\bar{\lambda}) &= \tfrac{1}{(2+\bar{\lambda})^2} - \bar{\lambda}^2 + (1+\bar{\lambda}).\Big[0.109 + 0.217(\bar{\lambda} - 0.15)^2\Big] \quad \text{if} \quad \bar{\lambda} \in [-1, 0.6378] \\ g(\bar{\lambda}) &= 0 \quad \text{otherwise} \\ \bar{\lambda} &= (\lambda_m + \mu_z)/(v_h/V_{MRref}) \\ \bar{\mu_{xy}} &= \mu_{xy}/(v_h/V_{MRref}) \end{aligned} \tag{17}$$

From Eq (14) - Eq (15), we can now derive an approximated and simplified expression for the static uniform inflow, in which we have assumed the longitudinal rotor TPP tilt angle to be small $\beta_{1c} \simeq 0$, we get

$$\begin{aligned} v_{i_o} &= A.C/(1 - B.C) \\ C &= -G_{eff}/(2V_T).V_{MRref} \end{aligned} \tag{18}$$

Finally, the ground effect correction factor is given from Ref. 68 as

$$G_{eff} = \frac{1}{0.9926 + 0.0379(2R_{rot}/h_H)^2} \tag{19}$$

III.B.3. Tip-Path-Plane (TPP) Angles

As for the Tip-Path-Plane (TPP) model, here too we assume a static behavior. The model is a simplified[p] implementation of the expressions presented in Ref. 53, 54. In particular we neglect the effect of roll, pitch and vertical accelerations on the rotor TPP angles.

[p] We do not use the wind-axis formalism of Ref. 53, 54

$$\begin{pmatrix} \beta_0 \\ -\beta_{1c} \\ -\beta_{1s} \end{pmatrix} = \mathbb{K}^{-1}.\left[\mathbb{F}_\theta.\begin{pmatrix} \theta_0 \\ -\theta_{1c}+\Theta_{MRc} \\ -\theta_{1s}+\Theta_{MRs} \end{pmatrix} + \mathbb{F}_{pq}.\begin{pmatrix} p \\ q \end{pmatrix} + \lambda.\mathbb{F}_\lambda + \mathbb{F}_0\right] \tag{20}$$

With the rotor total inflow expressed by

$$\lambda = (-V_{a,MR_w} + v_{i_o})/V_{MRref} \tag{21}$$

And the matrices $\mathbb{K}$, $\mathbb{F}_\theta$, $\mathbb{F}_{pq}$, $\mathbb{F}_\lambda$, and $\mathbb{F}_0$ given by

$$\mathbb{K} = \Omega_{MR}^2.\begin{bmatrix} P^2 & F_1.\mu_{xy} & 0 \\ F_2.\mu_{xy} & P^2-1 & G_1 \\ 0 & -G_1 & P^2-1 \end{bmatrix} \tag{22}$$

$$\mathbb{F}_\theta = \Omega_{MR}^2.\begin{bmatrix} G_2 & 0 & F_2.\mu_{xy} \\ 0 & G_2 & 0 \\ F_2.\mu_{xy} & 0 & G_2 \end{bmatrix} \tag{23}$$

Where we modified the element $\mathbb{F}_\theta(3,1)$, in Eq (23) compared to Ref. 53,54, since this gives better results. The remaining matrices are given by

$$\mathbb{F}_{pq} = \Omega_{MR}.\begin{bmatrix} -F_3.\mu_{xy} & 0 \\ H_1+\Theta_{MRp1} & -H_2+\Theta_{MRq1} \\ H_2+\Theta_{MRp2} & H_1+\Theta_{MRq2} \end{bmatrix} \tag{24}$$

$$\mathbb{F}_\lambda = \Omega_{MR}^2.\begin{bmatrix} G_3 \\ 0 \\ F_4.\mu_{xy} \end{bmatrix} \tag{25}$$

$$\mathbb{F}_0 = \begin{bmatrix} -C_0/I_b.g \\ 0 \\ 0 \end{bmatrix} \tag{26}$$

With

$$P^2 = 1 + K_{S_\beta}/(I_b.\Omega_{MR}^2) + \Delta_e/I_b.C_0 \tag{27a}$$
$$F_1 = -\epsilon/8.\gamma \tag{27b}$$
$$F_2 = -1/2(1/3-\epsilon/2).\gamma \tag{27c}$$
$$F_3 = 1/8(2/3-\epsilon).\gamma \tag{27d}$$
$$F_4 = -1/2(1/2-\epsilon).\gamma \tag{27e}$$
$$G_1 = 1/2(1/4-2/3\epsilon).\gamma \tag{27f}$$
$$G_2 = 1/2(1/4-1/3\epsilon).\gamma \tag{27g}$$
$$G_3 = 1/2(1/3-1/2\epsilon).\gamma \tag{27h}$$
$$H_1 = 2(1+\Delta_e/I_b.C_0) \tag{27i}$$
$$H_2 = 1/2(1/4-1/3.\epsilon).\gamma \tag{27j}$$

III.B.4. Forces

The rotor force coefficients, in the Hub-Body wind-axis frame F_{HBw} are given in Ref. 59. We did not use the side-force coefficient from Ref. 59 since it did not provide satisfactory results (when our model was compared with an equivalent FLIGHTLAB® model). For the drag, and thrust coefficients we have

$$C_{H_{MR}}^{HBw} = \frac{\sigma_{MR}.CD_{MR}}{8}.\left(3\mu_{xy} + 1.98\mu_{xy}^{2.7}\right) + \frac{\sigma_{MR}.CL_{MR_\alpha}}{2}.\left(\frac{\theta_0}{2}.\mu_{xy}.\lambda - \frac{\theta_{1c}.\beta_0}{6} + \frac{\theta_{1s}}{4}.\lambda + \frac{\mu_{xy}.\beta_0^2}{4}\right) \quad (28)$$

$$C_{T_{MR}}^{HBw} = -\frac{\sigma_{MR}.CL_{MR_\alpha}}{2}.\left(\frac{\theta_0}{3}.\left[B^3 + \frac{3}{2}B.\mu_{xy}^2\right] - \frac{B^2}{2}.\left[\lambda - \mu_{xy}.(\beta_{1c} + \theta_{1s})\right]\right) \quad (29)$$

Which gives in the body frame F_b

$$\begin{pmatrix} C_{H\,MR} \\ C_{Y\,MR} \\ C_{T\,MR} \end{pmatrix}^b = \mathbb{T}_{b(HBw)}.\begin{pmatrix} C_{H\,MR} \\ 0 \\ C_{T\,MR} \end{pmatrix}^{HBw} \quad (30)$$

With

$$\mathbb{T}_{b(HBw)} = \mathbb{T}_{b(HB)}.\mathbb{T}_{HB(HBw)} \quad (31)$$

Now since the main rotor shaft tilt angle is zero, the Hub-Body frame F_{HB} and the vehicle body frame F_b are identical, i.e. $\mathbb{T}_{b(HB)} = \mathbb{I}$. And

$$\mathbb{T}_{(HB)(HBw)} = \begin{pmatrix} -\cos\beta_{MR} & -\sin\beta_{MR} & 0 \\ -\sin\beta_{MR} & \cos\beta_{MR} & 0 \\ 0 & 0 & 1 \end{pmatrix} \quad (32)$$

The main rotor sideslip angle is expressed from the fuselage sideslip angle Eq (57) as

$$\beta_{MR} = \mod\left(\beta_F, 2\pi\right) \quad (33)$$

Finally expressing the main rotor forces in the body frame we get

$$\begin{pmatrix} F_{x_{MR}} \\ F_{y_{MR}} \\ F_{z_{MR}} \end{pmatrix}^b = \begin{pmatrix} C_{H\,MR} \\ C_{Y\,MR} \\ C_{T\,MR} \end{pmatrix}^b .\rho.\pi.R_{rot}^2.V_{MRref}^2 \quad (34)$$

III.B.5. Moments

The roll and pitch moments due to the flap hinge spring are given as in Ref. 59

$$L^b_{(MR,flap)} = -\frac{1}{1-\frac{\Delta_e}{R_{rot}}}.\frac{N_b}{2}.K_{S_\beta}.\Gamma.\beta_{1s} \tag{35a}$$

$$M^b_{(MR,flap)} = -\frac{1}{1-\frac{\Delta_e}{R_{rot}}}.\frac{N_b}{2}.K_{S_\beta}.\beta_{1c} \tag{35b}$$

The inertia roll and pitch moments, which arise when the plane of a rotor with offset hinges is tilted relative to the shaft, are given as in Ref. 60

$$L^b_{(MR,inertial)} = -\frac{N_b}{2}.M_{bl}.\Delta_e.y_{G_{bl}}.\Omega^2_{MR}.\Gamma.\beta_{1s} \tag{36a}$$

$$M^b_{(MR,inertial)} = -\frac{N_b}{2}.M_{bl}.\Delta_e.y_{G_{bl}}.\Omega^2_{MR}.\beta_{1c} \tag{36b}$$

For the main rotor torque (i.e. yaw moment), we simplify the description by only considering the induced and profile components of a rotor in vertical flight,[59] hence omitting forward flight components

$$N^b_{(MR,aero)} = \Gamma.\Big(-\lambda.C_{TMR} + \sigma_{MR}.CD_{MR}/8.\Big[1+4.6\mu^2_{xy}\Big]\Big).\rho.\pi.R^3_{rot}.V^2_{MRref} \tag{37}$$

Next, and by adding the main rotor forces times the respective moment arms, we obtain the total main rotor moments as

$$\begin{pmatrix} M_{x_{MR}} \\ M_{y_{MR}} \\ M_{z_{MR}} \end{pmatrix}^b = \begin{pmatrix} L_{(MR,flap)} + L_{(MR,inertial)} + y_H.F_{z_{MR}} - z_H.F_{y_{MR}} \\ M_{(MR,flap)} + M_{(MR,inertial)} + z_H.F_{x_{MR}} - x_H.F_{z_{MR}} \\ N_{(MR,aero)} + x_H.F_{y_{MR}} - y_H.F_{x_{MR}} \end{pmatrix}^b \tag{38}$$

III.B.6. Rotor RPM Dynamics

The main rotor RPM dynamics is related to the available and required power by the following expression[63]

$$N_b.I_b.\Omega_{MR}.\dot{\Omega}_{MR} = P_{shaft} - P_{req} \tag{39}$$

With P_{shaft} the available shaft power, and P_{req} the required power to keep the vehicle aloft. This latter is the sum of main rotor induced and profile power, tail rotor induced and profile power, power plant transmission losses, vehicle parasite power (i.e. drag due to fuselage, landing skids, rotor hub, etc), and finally main rotor, tail rotor, and fuselage aerodynamic interference losses.[69]

Considering the case of an engine failure, a first-order response in P_{shaft} is generally assumed to represent the power decay for turboshaft engines,[70,71] we have

$$\dot{P}_{shaft} = -\frac{P_{shaft}}{\tau_p} \tag{40}$$

With τ_p a to-be-identified time constant. For the required power P_{req}, we simplify the model by only considering the contributions from the main rotor as

$$P_{MR} = \Theta_{MRpwr}.N_{(MR,aero)}.\Omega_{MR} \tag{41}$$

III.B.7. Main Rotor Black-Box Modeling

This main rotor model is a so-called grey-box model, since it includes the following tabulated empirical coefficients, which will be determined from experimental data in Section VIII. We have

$$CL_{MR_\alpha} = f(\mu_x, \mu_y) \tag{42a}$$
$$CD_{MR} = f(\mu_x, \mu_y) \tag{42b}$$
$$\Theta_{MRc} = f(\mu_x, \mu_y) \tag{42c}$$
$$\Theta_{MRs} = f(\mu_x, \mu_y) \tag{42d}$$
$$\Theta_{MRp1} = f(\mu_x) \tag{42e}$$
$$\Theta_{MRp2} = f(\mu_x) \tag{42f}$$
$$\Theta_{MRq1} = f(\mu_x) \tag{42g}$$
$$\Theta_{MRq2} = f(\mu_x) \tag{42h}$$
$$\Theta_{MRvrs} = f(\mu_z.V_{MRref}/v_h) \tag{42i}$$
$$\Theta_{MRpwr} = f(\mu_x) \tag{42j}$$

IV. Tail Rotor Modeling

IV.A. Assumptions

Structural simplifications

- The blade has zero twist, constant chord, zero sweep, and has constant thickness ratio.
- The blade is rigid, hence torsion is neglected.

Aerodynamics simplifications

- Linear lift with constant lift curve slope, and uniform induced flow over the rotor.
- Aerodynamic interference effects from the main rotor is neglected, although this may well be an over-simplification, for some flight conditions.[72,73] Similarly, the aerodynamic interference from the vertical tail (due to blockage) is also neglected.
- Compressibility, blade stall and viscous flow effects are disregarded.

Dynamical simplifications

- No blade dynamics and simplified inflow dynamics.
- Unsteady effects neglected.

IV.B. Modeling

The tail rotor is a powerful design solution for torque balance, directional stability and control of single main rotor helicopters. The theory we apply here is based on the work done by Bailey in Ref. 74. The model represents a standard approach towards tail rotor modeling, as implemented among others in Ref. 64, 75, 76.

IV.B.1. Velocities

The tail rotor hub aerodynamic velocity in the body frame is given by

$$\mathbf{V}^b_{a,TR} = \begin{pmatrix} V_{a,TR_u} \\ V_{a,TR_v} \\ V_{a,TR_w} \end{pmatrix}^b = \begin{pmatrix} u + (q - q_w).z_{TR} - (r - r_w).y_{TR} \\ v - (p - p_w).z_{TR} + (r - r_w).x_{TR} \\ w + (p - p_w).y_{TR} - (q - q_w).x_{TR} \end{pmatrix}^b - \begin{pmatrix} u_w \\ v_w \\ w_w \end{pmatrix}^b \tag{43}$$

In the tail rotor frame F_{TR} of Ref. 75, we have

$$\mathbf{V}_{a,TR}^{TR} = \begin{pmatrix} 1 & 0 & 0 \\ 0 & 0 & 1 \\ 0 & -1 & 0 \end{pmatrix} .\mathbf{V}_{a,TR}^{b} \tag{44}$$

The non-dimensional velocities in frame F_{TR} are expressed as follows

$$\mu_{TRx} = V_{a,MR_u}^{TR}/V_{TRref} \tag{45a}$$
$$\mu_{TRy} = V_{a,MR_v}^{TR}/V_{TRref} \tag{45b}$$
$$\mu_{TRz} = \Gamma.V_{a,MR_w}^{TR}/V_{TRref} \tag{45c}$$
$$\mu_{TRxy} = \sqrt{\mu_{TRx}^2 + \mu_{TRy}^2} \quad \text{and} \quad V_{TRref} = \Omega_{TR}.R_{rot_{TR}} \tag{45d}$$

IV.B.2. Inflow

The theory we apply here is based on the work done by Bailey in Ref. 74, implemented among others in Ref. 64, 75, 76. The model given in this paper is a simplified approach of the Bailey model. First, the tail rotor blade pitch is given by

$$\theta_{TR} = \theta_{0_{TR}} - T_{TR}.\frac{\partial \beta_{0_{TR}}}{\partial T_{TR}}.\tan\delta_{3_{TR}} + \theta_{bias_{TR}} \tag{46}$$

The Bailey coefficients are given next by

$$t_1 = \frac{B_{TR}^2}{2} + \frac{\mu_{TRxy}^2}{4} \tag{47a}$$
$$t_2 = \frac{B_{TR}^3}{3} + \frac{B_{TR}.\mu_{TRxy}^2}{2} \tag{47b}$$

Assuming zero twist for the tail rotor blades, the inflow is then derived using momentum theory

$$\lambda_{dw} = \frac{CL_{TR_\alpha}.\sigma_{TR}}{2}.\left(\frac{\mu_{TRz}.t_1 + \theta_{TR}.t_2}{2\sqrt{\mu_{TRxy}^2 + \lambda_{TR}^2} + \frac{CL_{TR_\alpha}.\sigma_{TR}}{2}.t_1}\right) \tag{48}$$

And the total tail rotor inflow is given by

$$\lambda_{TR} = \lambda_{dw} - \mu_{TRz} \tag{49}$$

Where it is common practice to iterate between Eq (48) and Eq (49) until convergence within a reasonable tolerance. Once the final value of the tail rotor inflow λ_{dw_F} has been obtained, two form factors on roll and yaw rate are added to the inflow value as follows

$$\lambda_{dw} = \lambda_{dw_F} + \Theta_{TRp}.p + \Theta_{TRr}.r \tag{50}$$

IV.B.3. Forces

The tail rotor thrust is given by

$$T_{TR} = 2/K_{TR_{corr}}.\lambda_{dw}.\sqrt{\mu_{TRxy}^2 + \lambda_{TR}^2}.\rho.\pi.\left(\Omega_{TR}.R_{rot_{TR}}^2\right)^2 \tag{51}$$

Finally in the body frame we have

$$\begin{pmatrix} F_{x_{TR}} \\ F_{y_{TR}} \\ F_{z_{TR}} \end{pmatrix}^b = \begin{pmatrix} 0 \\ \Gamma.T_{TR} \\ 0 \end{pmatrix} \tag{52}$$

Where we have neglected any aerodynamic interference effects with the main rotor and vertical tail (e.g. blockage effect).

IV.B.4. Moments

The tail rotor moments are primarily due to the tail rotor force times the respective moment arms. For completeness we also add the rotor torque acting on the pitch axis,[59] we get

$$\begin{pmatrix} M_{x_{TR}} \\ M_{y_{TR}} \\ M_{z_{TR}} \end{pmatrix}^b = \begin{pmatrix} -z_{TR}.T_{TR} \\ \sigma_{TR}.CD_{TR}/8.(1 + 4.6\mu_{TRxy}^2).\rho.\pi.\Omega_{TR}^2.R_{rot_{TR}}^5 \\ x_{TR}.T_{TR} \end{pmatrix} \tag{53}$$

IV.B.5. Tail Rotor Black-Box Modeling

This tail rotor model is a so-called grey-box model, since it includes the following tabulated empirical coefficients, which will be determined from experimental data in Section VIII. We have

$$\Theta_{TRp} = f(\mu_x) \tag{54a}$$
$$\Theta_{TRr} = f(\mu_x) \tag{54b}$$

V. Fuselage Modeling

The flow around the fuselage is characterized by strong nonlinearities, and is further distorted by the influence of the main rotor wake. Hence, the associated forces and moments, due to the surface pressures and skin friction, are complex functions of flight speed and direction.[57] Indeed, it is well-known that important unsteady separation effects exist, but are rather complex to model.[57]

V.A. Assumptions

Aerodynamics Simplifications

- Fuselage aerodynamic center collocated with vehicle CG.
- Effect of rotor downwash on fuselage is neglected. It can however be modeled as in Ref. 77, using a polynomial in wake skew angle, where the polynomial coefficients need to be fit from flight data.[78]
- Only steady airloads effects on the fuselage are considered.

V.B. Modeling

The fuselage model is based upon aerodynamic lift and drag coefficients, which are tabulated as a function of airflow angle of attack and sideslip angles. For low speed sideways flight, the important fuselage characteristics are in general, the sideforce, vertical drag, and yawing moment. While in forward flight, the three most important characteristics include drag, and pitching and yawing moments variations with incidence and sideslip.[57] The fuselage rolling moment is usually small, except for configurations with deep hulls where the fuselage aerodynamic center may be significantly below the vehicle CG.[57] For additional information, see also Ref. 43, 79.

V.B.1. Velocities And Airflow Angles

The fuselage aerodynamic velocity, at its aerodynamic center, in the body frame is given by

$$\mathbf{V}^b_{a,F} = \begin{pmatrix} V_{a,F_u} \\ V_{a,F_v} \\ V_{a,F_w} \end{pmatrix}^b = \begin{pmatrix} u + (q - q_w).z_F - (r - r_w).y_F \\ v - (p - p_w).z_F + (r - r_w).x_F \\ w + (p - p_w).y_F - (q - q_w).x_F \end{pmatrix}^b - \begin{pmatrix} u_w \\ v_w \\ w_w \end{pmatrix}^b \tag{55}$$

The fuselage angle of attack is given by

$$\alpha_F = \arctan(V_{a,F_w}/|V_{a,F_u}|) \tag{56}$$

And the fuselage sideslip angle is given as in Ref. 55 by

$$\begin{array}{rcl} \beta_F & = & \arcsin(V_{a,F_v}/V_{a,F}) \quad \text{if} \quad V_{a,F_u} \geq 0 \\ \beta_F & = & \pi/2 + \arccos(V_{a,F_v}/V_{a,F}) \quad \text{if} \quad V_{a,F_u} < 0 \quad \text{and} \quad V_{a,F_v} \geq 0 \\ \beta_F & = & -\pi/2 - \arccos(-V_{a,F_v}/V_{a,F}) \quad \text{if} \quad V_{a,F_u} < 0 \quad \text{and} \quad V_{a,F_v} < 0 \end{array} \tag{57}$$

With $V_{a,F} = \sqrt{V^2_{a,F_u} + V^2_{a,F_v} + V^2_{a,F_w}}$.

V.B.2. Forces

In the body frame F_b we have

$$\begin{array}{rcl} F^b_{x_F} & = & q_{dp}.Cx^b_F(\alpha_F, \beta_F) \\ F^b_{y_F} & = & q_{dp}.Cy^b_F(\alpha_F, \beta_F) \\ F^b_{z_F} & = & q_{dp}.Cz^b_F(\alpha_F, \beta_F) \\ q_{dp} & = & 1/2.\rho.S_{ref_F}.V^2_{a,F} \end{array} \tag{58}$$

The aerodynamic coefficients $Cx_F(.)$, $Cy_F(.)$, and $Cz_F(.)$ are tabulated as a function of airflow angle of attack α_F, and sideslip angle β_F. These lookup tables have been derived from a scaled-down full-size helicopter fuselage aerodynamic model.

V.B.3. Moments

In the body frame F_b we have

$$\begin{array}{lcl} M^b_{x_F} & = & q_{dp}.Mx_F(\alpha_F,\beta_F).L_{ref_F} \\ M^b_{y_F} & = & q_{dp}.My_F(\alpha_F,\beta_F).L_{ref_F} \\ M^b_{z_F} & = & q_{dp}.Mz_F(\alpha_F,\beta_F).L_{ref_F} \\ q_{dp} & = & 1/2.\rho.S_{ref_F}.V^2_{a,F} \end{array} \tag{59}$$

Here too, the aerodynamic coefficients $Mx_F(.)$, $My_F(.)$, and $Mz_F(.)$ are tabulated as a function of airflow angle of attack α_F, and sideslip angle β_F. These lookup tables have also been derived from a scaled-down full-size helicopter fuselage aerodynamic model.

VI. Vertical Tail Modeling

The role of the vertical tail is twofold: (i) in forward flight, it generates a sideforce and yawing moment, hence reducing the tail rotor thrust requirement, in order to increase the fatigue life of the tail rotor,[57,63] and (ii) during maneuvers, and during wind gusts, it provides yaw damping and stiffness, enhancing directional stability.[57]

VI.A. Assumptions

Aerodynamics Simplifications

- Effect of main rotor downwash on vertical tail is neglected. It can however be modeled by using flat vortex wake theory[80] (valid for small sideslip angles), as presented in Ref. 81,82, or it may be modeled as a polynomial in wake skew angle as in Ref. 77.
- As an aside, the effect of the main rotor downwash on the tail boom is neglected, but ought to be considered at low speed, since it may influence yaw damping.[57]

VI.B. Modeling

The vertical tail is basically a wing,[61,62] several modeling approaches can be found in Ref. 43, 64, 77, 79. Here, we use a flat plate representation.

VI.B.1. Velocities and airflow angles

The vertical tail aerodynamic velocity, at its aerodynamic center, in the body frame is given by

$$\mathbf{V}^b_{a,VT} = \begin{pmatrix} V_{a,VT_u} \\ V_{a,VT_v} \\ V_{a,VT_w} \end{pmatrix}^b = \begin{pmatrix} u+(q-q_w).z_{VT}-(r-r_w).y_{VT} \\ v-(p-p_w).z_{VT}+(r-r_w).x_{VT} \\ w+(p-p_w).y_{VT}-(q-q_w).x_{VT} \end{pmatrix}^b - \begin{pmatrix} u_w \\ v_w \\ w_w \end{pmatrix}^b \tag{60}$$

Since in the sequel we will neglect the spanwise flow (along the z-axis), we have $V_{a,VT} = \sqrt{V^2_{a,VT_u} + V^2_{a,VT_v}}$.

And the vertical tail angle of attack is given by

$$\begin{array}{lcl} \alpha_{VT} & = & -\arctan(V_{a,VT_v}/V_{a,VT_u}) \quad \text{if} \quad V_{a,VT_u} \geq 0 \\ \alpha_{VT} & = & -\pi/2+\arctan(V_{a,VT_u}/V_{a,VT_v}) \quad \text{if} \quad V_{a,VT_u} < 0 \quad \text{and} \quad V_{a,VT_v} \geq 0 \\ \alpha_{VT} & = & \pi/2+\arctan(V_{a,VT_u}/V_{a,VT_v}) \quad \text{if} \quad V_{a,VT_u} < 0 \quad \text{and} \quad V_{a,VT_v} < 0 \end{array} \tag{61}$$

VI.B.2. Forces

In the body frame F_b we have

$$\begin{array}{lcl} F^b_{x_{VT}} & = & q_{dp}.Cx_{VT}(CL, CD, \alpha_{VT}) \\ F^b_{y_{VT}} & = & q_{dp}.Cy_{VT}(CL, CD, \alpha_{VT}) \\ F^b_{z_{VT}} & = & 0 \\ q_{dp} & = & 1/2.\rho.S_{ref_{VT}}.V^2_{a,VT} \end{array} \tag{62}$$

The aerodynamic coefficients $Cx_{VT}(.)$ and $Cy_{VT}(.)$ are first functions of the lift $CL(.)$ and drag $CD(.)$ aerodynamic coefficients of a flat plate. Additionally the $Cx_{VT}(.)$ and $Cy_{VT}(.)$ coefficients are also functions of the airflow angle of attack α_{VT}, through the aerodynamic forces projection on the body frame F_b. Further the $CL(.)$ and drag $CD(.)$ coefficients are also tabulated as a function of airflow angle of attack and Mach number.

VI.B.3. Moments

The vertical tail moments are due to the tail forces times the respective moment arms, and to the aerodynamic pitch moment of a flat plate. This aerodynamic moment produces a yaw moment about the vehicle CG. In the body frame F_b we have

$$\begin{array}{lcl} M^b_{x_{VT}} & = & -z_{VT}.F_{y_{VT}} \\ M^b_{y_{VT}} & = & z_{VT}.F_{x_{VT}} \\ M^b_{z_{VT}} & = & x_{VT}.F_{y_{VT}} - y_{VT}.F_{x_{VT}} + q_{dp}.Mz_{VT}.L_{ref_{VT}} \\ q_{dp} & = & 1/2.\rho.S_{ref_{VT}}.V^2_{a,VT} \end{array} \tag{63}$$

Here the aerodynamic coefficient $Mz_{VT}(.)$ represents the pitch aerodynamic coefficient of a flat plate. This latter coefficient is tabulated as a function of airflow angle of attack and Mach number.

VII. Horizontal Tail Modeling

The role of the horizontal tail is also twofold: (i) in forward flight, it generates a trim load that reduces the main rotor fore-aft flapping, and (ii) during maneuvers, and during wind gusts, it provides pitch damping and stiffness, enhancing pitch stability.[57]

VII.A. Assumptions

Aerodynamics Simplifications

- Effect of main rotor downwash on horizontal tail is neglected. Again it can be modeled by using flat vortex wake theory[80] (valid for small sideslip angles), as presented in Ref. 81,82, or it may be modeled as a polynomial in wake skew angle as in Ref. 77.

VII.B. Modeling

Here too, we use a flat plate representation. Again, more sophisticated models exist,[61,62] and several approaches can be found in Ref. 43,64,77,79. It is also well-known that, depending on the longitudinal and vertical position of the horizontal tail with respect to the main rotor, erratic longitudinal trim shifts may happen when the helicopter is transitioning from hover to forward flight,[63] as the main rotor wake impinges on the tail surface.[57]

VII.B.1. Velocities And Airflow Angles

The horizontal tail aerodynamic velocity, at its aerodynamic center, in the body frame is given by

$$\mathbf{V}^b_{a,HT} = \begin{pmatrix} V_{a,HT_u} \\ V_{a,HT_v} \\ V_{a,HT_w} \end{pmatrix}^b = \begin{pmatrix} u + (q - q_w).z_{HT} - (r - r_w).y_{HT} \\ v - (p - p_w).z_{HT} + (r - r_w).x_{HT} \\ w + (p - p_w).y_{HT} - (q - q_w).x_{HT} \end{pmatrix}^b - \begin{pmatrix} u_w \\ v_w \\ w_w \end{pmatrix}^b \tag{64}$$

Since in the sequel we will neglect the spanwise flow (along the y-axis), we have $V_{a,HT} = \sqrt{V^2_{a,HT_u} + V^2_{a,HT_w}}$.

And the horizontal tail angle of attack is given by

$$\begin{array}{rcl} \alpha_{HT} & = & \arctan(V_{a,HT_w}/V_{a,HT_u}) \quad \text{if} \quad V_{a,HT_u} \geq 0 \\ \alpha_{HT} & = & \pi/2 + \arctan(-V_{a,HT_u}/V_{a,HT_w}) \quad \text{if} \quad V_{a,HT_u} < 0 \quad \text{and} \quad V_{a,HT_w} \geq 0 \\ \alpha_{HT} & = & -\pi/2 - \arctan(V_{a,HT_u}/V_{a,HT_w}) \quad \text{if} \quad V_{a,HT_u} < 0 \quad \text{and} \quad V_{a,HT_w} < 0 \end{array} \tag{65}$$

VII.B.2. Forces

In the body frame F_b we have

$$\begin{array}{rcl} F^b_{x_{HT}} & = & q_{dp}.Cx_{HT}(CL, CD, \alpha_{HT}) \\ F^b_{y_{HT}} & = & 0 \\ F^b_{z_{HT}} & = & q_{dp}.Cz_{HT}(CL, CD, \alpha_{HT}) \\ q_{dp} & = & 1/2.\rho.S_{ref_{HT}}.V^2_{a,HT} \end{array} \tag{66}$$

Again, the aerodynamic coefficients $Cx_{HT}(.)$ and $Cz_{HT}(.)$ are first functions of the lift $CL(.)$ and drag $CD(.)$ aerodynamic coefficients of a flat plate. Additionally the $Cx_{HT}(.)$ and $Cz_{HT}(.)$ coefficients are also functions of the airflow angle of attack α_{HT}, through the aerodynamic forces projection on the body frame F_b. Further the $CL(.)$ and drag $CD(.)$ coefficients are also tabulated as a function of airflow angle of attack and Mach number.

VII.B.3. Moments

The horizontal tail moments are first due to the tail forces times the respective moment arms, and further are also due to the aerodynamic pitch moment of a flat plate. This aerodynamic moment produces a pitch moment about the vehicle CG. In the body frame F_b we have

$$\begin{array}{rcl} M^b_{x_{HT}} & = & y_{HT}.F_{z_{HT}} \\ M^b_{y_{HT}} & = & z_{HT}.F_{x_{HT}} - x_{HT}.F_{z_{HT}} + q_{dp}.My_{HT}.L_{ref_{HT}} \\ M^b_{z_{HT}} & = & -y_{HT}.F_{x_{HT}} \\ q_{dp} & = & 1/2.\rho.S_{ref_{HT}}.V^2_{a,HT} \end{array} \tag{67}$$

Here too the aerodynamic coefficient $My_{HT}(.)$ represents the pitch aerodynamic coefficient of a flat plate. This latter coefficient is tabulated as a function of airflow angle of attack and Mach number.

VIII. Black-Box Modeling

VIII.A. The Multiple-Model Approach

As mentioned in Section I.A, the purpose of the black-box model is to replace not sufficiently well understood and/or computationally intensive areas of a white-box model, by a much simpler, yet empirical, representation. Here the modus operandi of our approach consists in decomposing the system's full operational range into a number of possibly overlapping operating regimes,[2,83] with each operating regime being described by a single local nonlinear model. In our case, the black-box model may be viewed as a unit accepting inputs, the so-called scheduling variables, which should characterize and capture these operating regimes,[84,85] whereas its outputs compensate for the un-modeled dynamics and/or un-modeled nonlinearities. Then, a method for combining the local models into a global one must be devised. For this purpose, numerous strategies have been developed, such as deterministic vs stochastic, and soft vs hard partitioning.[2,83] For example, in a stochastic or probabilistic approach, statistical methods are used to infer which operating regime is most appropriate, at a particular time. This approach is based upon the associated model probability density, indicating the level of model correctness.[83] Further, in soft partitioning, one assumes that the model behavior changes gradually as the operating point moves between different operating regimes. Here smooth deterministic transitions between local models may be implemented via fuzzy logic or interpolation methods.[83] Finally, for the case of so-called hard partitioning, which refers to non-smooth systems exhibiting abrupt changes in behavior or mechanisms (e.g. jump phenomena, bifurcations), a framework based upon discrete logic, decision trees, and/or hybrid systems may be most appropriate.

VIII.B. Black-Box: Modeling Framework

The black-box model used here generates the following twelve coefficients (see also Appendix A)

- Two main rotor aerodynamic coefficients (CL_{MR_α}, CD_{MR}), see Eq (28), Eq (29), and Eq (37)
- Eight main rotor empirical coefficients ($\Theta_{MRc}, \Theta_{MRs}, \Theta_{MRp1}, \Theta_{MRp2}, \Theta_{MRq1}, \Theta_{MRq2}, \Theta_{MRvrs}, \Theta_{MRpwr}$), see Eq (16), Eq (20), Eq (24), and Eq (41)
- Two tail rotor empirical coefficients ($\Theta_{TRp}, \Theta_{TRr}$), see Eq (50)

The number, and *"location"*, of these coefficients within the white-box model structure, have been decided through engineering judgment. Next, we assume that the presence of these coefficients allows for a versatile enough modeling framework, which permits us to conjecture that the true system is believed to be inside the representation capacity of this preliminary modeling structure. What then remains to be defined are: (i) the selection of the scheduling variables, (ii) the selection of the operating regimes, (iii) the experiment design that will, among others, delineate the nature and amount of data available for the subsequent (iv) coefficients estimation process.

Now the first and third items, listed above, are intrinsically related by the trade-off between the conflicting requirements of having a small approximation error together with a small estimation error, in other words the well-known bias-variance trade-off in the fields of statistics and system identification.[3,86] On the one hand, if the system is assumed to be outside the representation capacity of the selected model set, which for example may be true in case of a too restrictive scheduling variables set, an error between the system and its model will exist, even if an infinite data set is made available.[3] On the other hand, the effect of noisy measurements and/or the obvious fact that one does not have access to an infinite amount of data, will always result in a certain level of estimation error.

Besides this bias-variance trade-off constraint, there is another difficulty related to the lowering of the approximation error. An inherent issue with functions approximation approaches, based upon function's domain partitioning, is the famous curse of dimensionality.[83] Indeed, with an increasing number of scheduling variables, the number of partitions required will increase exponentially.[87] Hence, to avoid such a problem while accepting a higher bias error, we chose to have the here above listed coefficients depend upon only one or two scheduling variables, chosen from the set of vehicle advance ratios μ, along the x, y, and/or z directions, see Eq (42) and Eq (54).

For the selection of the operating regimes, it is intuitively clear that their total number will depend on the dynamical and smoothness nature of the system, and the dimensionality, of the operating space.[3] In other words the lower the number of operating regimes, the lower the level of overlap between local models. This may be an acceptable approach for systems with slowly varying and smooth properties. Whereas for non-smooth systems and/or in the event of rapidly varying physical phenomena, e.g. flight within the Vortex-Ring-State (VRS), a much denser grid of the system's full operational range may be required.[2] Then comes the question of uniform [q] vs nonuniform partitioning. While the uniform approach is simpler to implement, it is probably undesirable and unrealistic for anything else than low complexity problems.[87] For our model, which is highly nonlinear and rapidly varying, we opted for a somewhat denser grid, with uniform partitioning in the range[r] of 1 to 2.5 m/s[s]. This form of partitioning was affordable since we chose a very small number of scheduling variables.

Concerning now the determination of the global model from the local nonlinear ones, and with the view of using the most straightforward approach, we apply a deterministic soft partitioning approach, based upon simple linear interpolation between operating regimes. Here we assume that the helicopter dynamics have sufficiently smooth properties, which is a reasonable assumption, except perhaps for the fuselage tabulated aerodynamic coefficients.

With regard to the paradigm of experiment design, which is also known as the science of optimal data collection,[83,86,88] an input signal has to be applied such that the measurements contain enough information to optimally estimate the black-box model coefficients. Often either a sine-sweep input signal,[89–92] or a small amplitude high frequency signal superimposed on a large amplitude low frequency signal, may contain sufficient information for the modeling task to be successful.[91,93] However, in this paper, we present only preliminary results, based upon a single frequency sinusoid of 1° in amplitude, at a frequency of 2 Hz, corresponding to the maximum anticipated closed-loop system bandwidth for autonomous flight.

For aspects related to the coefficients estimation process, these will be detailed in the next sections. In the sequel, the term *original model* refers to our helicopter dynamical model, with all empirical coefficients set to zero, $\Theta_{i i=1\ldots10} = 0$, and with constant values for the $(CL_{MR_\alpha}, CD_{MR})$ coefficients, derived from our previous work of Ref. 49–51. Since flight data was not available, the FLIGHTLAB non-linear simulation model was used as a proxy, albeit in a noise-free setting, for experimental data. Further, in this study, we have also made an extensive use of FLIGHTLAB, by using some model data which are generally not provided by a classical sensors suite, e.g. main rotor inflow is typically not measured on-board a helicopter UAV.

Finally, it could seem somewhat odd to identify a simpler grey-box model from another existing high-fidelity simulation model. Indeed such comprehensive and high-fidelity simulation models, such as FLIGHTLAB, would allow for the design of optimal trajectories that capture the fine-scale helicopter higher frequency phenomena, such as the main rotor blade flap-lag dynamics,[94] and main rotor dynamic inflow,[66,95] resulting in highly accurate trajectories. The two main drawbacks, related to the nonlinear optimal control framework, of using such models come from (i) the inherent numerical instabilities associated with the numerical optimizations, that tend to get exacerbated with the increase in model complexity, and (ii) the corresponding high computational cost[t], which may effectively preclude any further potential on-line use of the trajectory generation process, for real-time re-planning applications, albeit in a receding-horizon framework.

VIII.C. Improving The Static White-Box Behavior

First, to better match the FLIGHTLAB uniform inflow in the VRS, during a pure vertical descent, we added the empirical coefficient Θ_{MRvrs} in the main rotor inflow expression Eq (16). This coefficient is simply the ratio of experimental to modeled inflow in the VRS, scheduled along μ_z, at specified operating regimes P_n.

[q] Fixed step increments of the scheduling variables.
[r] Each scheduling variable has its own step size.
[s] We express in this paragraph the step size in a dimensional form, since it is easier to grasp.
[t] Although with the steady increase in computer power, use of the FLIGHTLAB software, as an embedded version, in a real-time planning application, may soon be feasible.

In addition, from the comparison of trim results between the original model and FLIGHTLAB, we concluded that the trim characteristics in roll/pitch/yaw and vertical channel needed to be improved. To enhance the yaw and vertical channels, we opted to have the main rotor lift curve slope $CL_{MR_\alpha}(\mu_x, \mu_y)$ and drag $CD_{MR}(\mu_x, \mu_y)$ depend upon vehicle longitudinal and lateral velocities, as scheduling variables. To improve the roll and pitch channels, we included two empirical coefficients in the TPP formulation, i.e. $\Theta_{MRc}(\mu_x, \mu_y)$ and $\Theta_{MRs}(\mu_x, \mu_y)$, depending upon the same scheduling variables, see Eq (20).

Next the estimation of these coefficients is given as follows. First, we partition the operating space in P_i trim operating regimes. For each P_i, obtain from FLIGHTLAB the corresponding state/input trim data $(\mathbf{x}_{Trim_i}, \mathbf{u}_{Trim_i})$. Then, the coefficients $\mathbf{V} = (CL_{MR_\alpha}\ CD_{MR}\ \Theta_{MRc}\ \Theta_{MRs})^T$, defined on the compact set $\mathcal{V}$, s.t. $\mathcal{V} \subset \mathbb{R}^4$, are obtained as the solution to a multi-objective, algebraic, nonlinear, constrained optimization problem, suched that

$$\mathbf{V}^* \triangleq \arg\min_{\mathbf{V}\in\mathcal{V}} J(\mathbf{V}) \quad \text{for each} \quad P_i \tag{68}$$

The goal of the multi-objective cost $J(.)$ is to minimize the following vehicle accelerations, i.e. achieving a trim flight in the roll/pitch/yaw and vertical channels

$$J(\mathbf{V}) = (|\dot{p}|\ |\dot{q}|\ |\dot{r}|\ |\dot{w}|)^T \tag{69}$$

With the additional state/input trim constraints

$$\begin{aligned} \mathbf{x} &= \mathbf{x}_{Trim_i} \quad \text{for each} \quad P_i \\ \mathbf{u} &= \mathbf{u}_{Trim_i} \end{aligned} \tag{70}$$

And

$$0 < \quad CL_{MR_\alpha} \quad \text{and} \quad 0 < CD_{MR} \tag{71}$$

This optimization can be solved through standard Sequential Quadratic Programming (SQP) algorithms,[96–98] e.g. with the MATLAB® function *fgoalattain* of the Optimization Toolbox.

Finally, since we omitted contributions due to forward flight when deriving an expression for the main rotor torque (i.e. yaw moment), we adjust the main rotor power by an empirical coefficient Θ_{MRpwr}, see Eq (41). This coefficient is simply the ratio of experimental power to modeled power, at selected P_j trim operating points along μ_x.

VIII.D. Improving The Dynamic White-Box Behavior

Once good results in terms of static behavior fidelity had been obtained, we compared the dynamic response to sinusoidal control inputs. Here, improvements in the roll/pitch and yaw channels were deemed necessary.

For better response in the roll/pitch channels, we introduced four empirical coefficients Θ_{MRp1}, Θ_{MRp2}, Θ_{MRq1}, and Θ_{MRq2} as a function of the μ_x scheduling variable, see Eq (24), and computed at P_k operating regimes. These coefficients were derived through linear Least Squares (LS),[99] in an equation-error identification framework.[88, 100] Technically these four empirical coefficients will impact the main rotor forces and moments, along the three axes. However, to simplify the derivations, and since from engineering judgment, we assume that their impact will primarily be on the roll/pitch axes, we decided to use only the $\dot{p}$ and $\dot{q}$ acceleration equations from Eq (4). The basic idea here, since these four coefficients appear linearly in these two acceleration equations, is to use these latter equations at each timestamp, with the following FLIGHTLAB data $(\phi, \theta, \psi, u, v, w, p, q, r, \dot{u}, \dot{v}, \dot{w}, \dot{p}, \dot{q}, \dot{r})^T$, and then let our model compute the forces and roll and pitch moments, in a way that minimizes residuals between the FLIGHTLAB and model $(\dot{p}, \dot{q})^T$, in a least-squares sense. We get

$$(\Theta_{MRp1}\ \Theta_{MRp2}\ \Theta_{MRq1}\ \Theta_{MRq2})^T = (A^T.A)^{-1}.A^T.Y \tag{72}$$

With the vector Y and matrix A given by

$$Y = \begin{bmatrix} Y_{roll_{MR}} \\ Y_{pitch_{MR}} \end{bmatrix} \tag{73}$$

$$A = \begin{bmatrix} roll_{MR_{C_1}} & roll_{MR_{C_2}} & roll_{MR_{C_3}} & roll_{MR_{C_4}} \\ pitch_{MR_{C_1}} & pitch_{MR_{C_2}} & pitch_{MR_{C_3}} & pitch_{MR_{C_4}} \end{bmatrix} \tag{74}$$

The definitions for $Y_{roll_{MR}}$ and $Y_{pitch_{MR}}$ are given hereunder, after some lengthy but straightforward algebraic manipulations, as

$$\begin{aligned} Y_{roll_{MR}} &= M_{exclMR_x,G_{Fus}} - (-1/2/(1-\Delta_e/R_{rot}).Nb.K_{S_\beta}.\Gamma.\beta_{1s_T} - 1/2.Nb.M_{bl}.\Delta_e.y_{G_{bl}}.\Omega^2_{MR}.\Gamma.\beta_{1s_T} \\ &+z_F.F^b_{Yaero,G_{Fus}} - y_F.(F^b_{ZexclMR,G_{Fus}} - 1/2.\sigma_{MR}.CL_{MR_\alpha}.(1/3.\theta_0.(B^3+3/2.B.\mu^2_{xy}) - 1/2.B^2. \\ &(\lambda-\mu_{xy}.(\beta_{1c_T}+\theta_{1s}))).\rho.\pi.R^2_{rot}.V^2_{MRref}) - zH.F^b_{y_{MR}} \\ &-1/2.yH.\sigma_{MR}.CL_{MR_\alpha}.(1/3.\theta_0.(B^3+3/2.B.\mu^2_{xy}) - 1/2.B^2.(\lambda-\mu_{xy}.(\beta_{1c_T}+\theta_{1s}))).\rho.\pi.R^2_{rot}.V^2_{MRref}) \end{aligned} \tag{75}$$

$$\begin{aligned} Y_{pitch_{MR}} &= M_{exclMR_y,G_{Fus}} - (-1/2/(1-\Delta_e/R_{rot}).Nb.K_{S_\beta}.\beta_{1c_T} - 1/2.Nb.M_{bl}.\Delta_e.y_{G_{bl}}.\Omega^2_{MR}.\beta_{1c_T} + zH.F^b_{x_{MR}} \\ &+1/2.xH.\sigma_{MR}.CL_{MR_\alpha}.(1/3.\theta_0.(B^3+3/2.B.\mu^2_{xy}) - 1/2.B^2.(\lambda-\mu_{xy}.(\beta_{1c_T}+\theta_{1s}))).\rho.\pi.R^2_{rot}.V^2_{MRref} \\ &-z_F.F^b_{XexclMR,G_{Fus}} + x_F.(F^b_{ZexclMR,G_{Fus}} - 1/2.\sigma_{MR}.CL_{MR_\alpha}. \\ &(1/3.\theta_0.(B^3+3/2.B.\mu^2_{xy}) - 1/2.B^2.(\lambda-\mu_{xy}.(\beta_{1c_T}+\theta_{1s}))).\rho.\pi.R^2_{rot}.V^2_{MRref})) \end{aligned} \tag{76}$$

Whereas the definitions for the first row of the A matrix are given by

$$\begin{aligned} roll_{MR_{C_1}} &= (-1/2/(1-\Delta_e/R_{rot}).Nb.K_{S_\beta}.\Gamma.\beta_{1s_{C1}} - 1/2.Nb.M_{bl}.\Delta_e.y_{G_{bl}}.\Omega^2_{MR}.\Gamma.\beta_{1s_{C1}} \\ &+1/4.y_F.\sigma_{MR}.CL_{MR_\alpha}.B^2.\mu_{xy}.\beta_{1c_{C1}}.\rho.\pi.R^2_{rot}.V^2_{MRref} - 1/4.yH.\sigma_{MR}.CL_{MR_\alpha}.B^2.\mu_{xy}.\beta_{1c_{C1}}.\rho.\pi.R^2_{rot}.V^2_{MRref}) \end{aligned} \tag{77}$$

$$\begin{aligned} roll_{MR_{C2}} &= (-1/2.Nb.M_{bl}.\Delta_e.y_{G_{bl}}.\Omega^2_{MR}.\Gamma.\beta_{1s_{C2}} + 1/4.y_F.\sigma_{MR}.CL_{MR_\alpha}.B^2.\mu_{xy}.\beta_{1c_{C2}}.\rho.\pi.R^2_{rot}.V^2_{MRref} \\ &-1/4.yH.\sigma_{MR}.CL_{MR_\alpha}.B^2.\mu_{xy}.\beta_{1c_{C2}}.\rho.\pi.R^2_{rot}.V^2_{MRref} - 1/2/(1-\Delta_e/R_{rot}).Nb.K_{S_\beta}.\Gamma.\beta_{1s_{C2}}) \end{aligned} \tag{78}$$

$$\begin{aligned} roll_{MR_{C3}} &= (-1/2/(1-\Delta_e/R_{rot}).Nb.K_{S_\beta}.\Gamma.\beta_{1s_{C3}} - 1/2.Nb.M_{bl}.\Delta_e.y_{G_{bl}}.\Omega^2_{MR}.\Gamma.\beta_{1s_{C3}} \\ &+1/4.y_F.\sigma_{MR}.CL_{MR_\alpha}.B^2.\mu_{xy}.\beta_{1c_{C3}}.\rho.\pi.R^2_{rot}.V^2_{MRref} - 1/4.yH.\sigma_{MR}.CL_{MR_\alpha}.B^2.\mu_{xy}.\beta_{1c_{C3}}.\rho.\pi.R^2_{rot}.V^2_{MRref}) \end{aligned} \tag{79}$$

$$\begin{aligned} roll_{MR_{C4}} &= (-1/2/(1-\Delta_e/R_{rot}).Nb.K_{S_\beta}.\Gamma.\beta_{1s_{C4}} + 1/4.y_F.\sigma_{MR}.CL_{MR_\alpha}.B^2.\mu_{xy}.\beta_{1c_{C4}}.\rho.\pi.R^2_{rot}.V^2_{MRref} \\ &-1/2.Nb.M_{bl}.\Delta_e.y_{G_{bl}}.\Omega^2_{MR}.\Gamma.\beta_{1s_{C4}} - 1/4.yH.\sigma_{MR}.CL_{MR_\alpha}.B^2.\mu_{xy}.\beta_{1c_{C4}}.\rho.\pi.R^2_{rot}.V^2_{MRref}) \end{aligned} \tag{80}$$

And the definitions for the second row of the A matrix are given by

$$pitch_{MR_{C_1}} = (-1/2/(1-\Delta_e/R_{rot}).Nb.K_{S_\beta}.\beta_{1c_{C1}} + 1/4.xH.\sigma_{MR}.CL_{MR_\alpha}.B^2.\mu_{xy}.\beta_{1c_{C1}}.\rho.\pi.R^2_{rot}.V^2_{MRref}$$
$$-1/2.Nb.M_{bl}.\Delta_e.y_{G_{bl}}.\Omega^2_{MR}.\beta_{1c_{C1}} - 1/4.x_F.\sigma_{MR}.CL_{MR_\alpha}.B^2.\mu_{xy}.\beta_{1c_{C1}}.\rho.\pi.R^2_{rot}.V^2_{MRref}) \tag{81}$$

$$pitch_{MR_{C2}} = (-1/2/(1-\Delta_e/R_{rot}).Nb.K_{S_\beta}.\beta_{1c_{C2}} - 1/2.Nb.M_{bl}.\Delta_e.y_{G_{bl}}.\Omega^2_{MR}.\beta_{1c_{C2}}$$
$$+1/4.xH.\sigma_{MR}.CL_{MR_\alpha}.B^2.\mu_{xy}.\beta_{1c_{C2}}.\rho.\pi.R^2_{rot}.V^2_{MRref} - 1/4.x_F.\sigma_{MR}.CL_{MR_\alpha}.B^2.\mu_{xy}.\beta_{1c_{C2}}.\rho.\pi.R^2_{rot}.V^2_{MRref}) \tag{82}$$

$$pitch_{MR_{C3}} = (-1/2/(1-\Delta_e/R_{rot}).Nb.K_{S_\beta}.\beta_{1c_{C3}} - 1/2.Nb.M_{bl}.\Delta_e.y_{G_{bl}}.\Omega^2_{MR}.\beta_{1c_{C3}}$$
$$+1/4.xH.\sigma_{MR}.CL_{MR_\alpha}.B^2.\mu_{xy}.\beta_{1c_{C3}}.\rho.\pi.R^2_{rot}.V^2_{MRref} - 1/4.x_F.\sigma_{MR}.CL_{MR_\alpha}.B^2.\mu_{xy}.\beta_{1c_{C3}}.\rho.\pi.R^2_{rot}.V^2_{MRref}) \tag{83}$$

$$pitch_{MR_{C4}} = (-1/2/(1-\Delta_e/R_{rot}).Nb.K_{S_\beta}.\beta_{1c_{C4}} + 1/4.xH.\sigma_{MR}.CL_{MR_\alpha}.B^2.\mu_{xy}.\beta_{1c_{C4}}.\rho.\pi.R^2_{rot}.V^2_{MRref}$$
$$-1/2.Nb.M_{bl}.\Delta_e.y_{G_{bl}}.\Omega^2_{MR}.\beta_{1c_{C4}} - 1/4.x_F.\sigma_{MR}.CL_{MR_\alpha}.B^2.\mu_{xy}.\beta_{1c_{C4}}.\rho.\pi.R^2_{rot}.V^2_{MRref}) \tag{84}$$

Where the following additional variables are defined as

$$\begin{pmatrix} \beta_{1c_{C1}} \\ \beta_{1c_{C2}} \\ \beta_{1c_{C3}} \\ \beta_{1c_{C4}} \end{pmatrix} = \begin{pmatrix} 1/\Omega_{MR}.P^2.(P^2-1)/(-P^6+2.P^4-P^2-P^2.G_1^2+F_2.\mu^2_{xy}.F_1.P^2-F_2.\mu^2_{xy}.F_1).p \\ 1/\Omega_{MR}.P^2.(P^2-1)/(-P^6+2.P^4-P^2-P^2.G_1^2+F_2.\mu^2_{xy}.F_1.P^2-F_2.\mu^2_{xy}.F_1).q \\ -1/\Omega_{MR}.P^2.G_1/(-P^6+2.P^4-P^2-P^2.G_1^2+F_2.\mu^2_{xy}.F_1.P^2-F_2.\mu^2_{xy}.F_1).p \\ -1/\Omega_{MR}.P^2.G_1/(-P^6+2.P^4-P^2-P^2.G_1^2+F_2.\mu^2_{xy}.F_1.P^2-F_2.\mu^2_{xy}.F_1).q \end{pmatrix} \tag{85}$$

$$\begin{pmatrix} \beta_{1s_{C1}} \\ \beta_{1s_{C2}} \\ \beta_{1s_{C3}} \\ \beta_{1s_{C4}} \end{pmatrix} = \begin{pmatrix} 1/\Omega_{MR}.P^2.G_1/(-P^6+2.P^4-P^2-P^2.G_1^2+F_2.\mu^2_{xy}.F_1.P^2-F_2.\mu^2_{xy}.F_1).p \\ 1/\Omega_{MR}.P^2.G_1/(-P^6+2.P^4-P^2-P^2.G_1^2+F_2.\mu^2_{xy}.F_1.P^2-F_2.\mu^2_{xy}.F_1).q \\ -1/\Omega_{MR}.(-P^4+P^2+F_2.\mu^2_{xy}.F_1)/(-P^6+2.P^4-P^2-P^2.G_1^2+F_2.\mu^2_{xy}.F_1.P^2-F_2.\mu^2_{xy}.F_1). \\ -1/\Omega_{MR}.(-P^4+P^2+F_2.\mu^2_{xy}.F_1)/(-P^6+2.P^4-P^2-P^2.G_1^2+F_2.\mu^2_{xy}.F_1.P^2-F_2.\mu^2_{xy}.F_1). \end{pmatrix} \tag{86}$$

$$\begin{aligned} \beta_{1c_T} = & -1/\Omega^2_{MR}.F_2.\mu_{xy}.(P^2-1)/(-P^6+2.P^4-P^2-P^2.G_1^2+F_2.\mu^2_{xy}.F_1.P^2-F_2.\mu^2_{xy}.F_1). \\ & (\Omega^2_{MR}.G_2.\theta_0+\Omega^2_{MR}.F_2.\mu_{xy}.B_{1c}-\Omega_{MR}.F_4.\mu_{xy}.p+\lambda.\Omega^2_{MR}.G_5-C_0/I_b.g) \\ & +1/\Omega^2_{MR}.P^2.(P^2-1)/(-P^6+2.P^4-P^2-P^2.G_1^2+F_2.\mu^2_{xy}.F_1.P^2-F_2.\mu^2_{xy}.F_1). \\ & (\Omega^2_{MR}.G_2.A_{1c}+\Omega_{MR}.H_1.p-\Omega_{MR}.H_2.q) \\ & -1/\Omega^2_{MR}.P^2.G_1/(-P^6+2.P^4-P^2-P^2.G_1^2+F_2.\mu^2_{xy}.F_1.P^2-F_2.\mu^2_{xy}.F_1). \\ & (\Omega^2_{MR}.F_2.\mu_{xy}.\theta_0+\Omega^2_{MR}.G_2.B_{1c}+\Omega_{MR}.H_2.p+\Omega_{MR}.H_1.q+\lambda.\Omega^2_{MR}.F_5.\mu_{xy}) \end{aligned} \tag{87}$$

$$\begin{aligned} \beta_{1s_T} = & -1/\Omega^2_{MR}.F_2.\mu_{xy}.G_1/(-P^6+2.P^4-P^2-P^2.G_1^2+F_2.\mu^2_{xy}.F_1.P^2-F_2.\mu^2_{xy}.F_1). \\ & (\Omega^2_{MR}.G_2.\theta_0+\Omega^2_{MR}.F_2.\mu_{xy}.B_{1c}-\Omega_{MR}.F_4.\mu_{xy}.p+\lambda.\Omega^2_{MR}.G_5-C_0/I_b.g) \\ & +1/\Omega^2_{MR}.P^2.G_1/(-P^6+2.P^4-P^2-P^2.G_1^2+F_2.\mu^2_{xy}.F_1.P^2-F_2.\mu^2_{xy}.F_1). \\ & (\Omega^2_{MR}.G_2.A_{1c}+\Omega_{MR}.H_1.p-\Omega_{MR}.H_2.q) \\ & -1/\Omega^2_{MR}.(-P^4+P^2+F_2.\mu^2_{xy}.F_1)/(-P^6+2.P^4-P^2-P^2.G_1^2+F_2.\mu^2_{xy}.F_1.P^2-F_2.\mu^2_{xy}.F_1). \\ & (\Omega^2_{MR}.F_2.\mu_{xy}.\theta_0+\Omega^2_{MR}.G_2.B_{1c}+\Omega_{MR}.H_2.p+\Omega_{MR}.H_1.q+\lambda.\Omega^2_{MR}.F_5.\mu_{xy}) \end{aligned} \tag{88}$$

$$F^b_{ZexclMR,G_{Fus}} = F^b_{z_{TR}} + F^b_{z_F} + F^b_{z_{VT}} + F^b_{z_{HT}} \tag{89}$$

$$\mathbf{M}^b_{exclMR,G_{Fus}} = \begin{pmatrix} M_{exclMR_x,G_{Fus}} \\ M_{exclMR_y,G_{Fus}} \\ M_{exclMR_z,G_{Fus}} \end{pmatrix}^b = \mathbb{I}_{Fus}.\begin{pmatrix} \dot{p} \\ \dot{q} \\ \dot{r} \end{pmatrix}^b + \begin{pmatrix} p \\ q \\ r \end{pmatrix}^b \times \left[\mathbb{I}_{Fus}.\begin{pmatrix} p \\ q \\ r \end{pmatrix}^b\right] - \left[\begin{pmatrix} M_{x_{TR}} \\ M_{y_{TR}} \\ M_{z_{TR}} \end{pmatrix}^b + \begin{pmatrix} M_{x_F} \\ M_{y_F} \\ M_{z_F} \end{pmatrix}^b + \begin{pmatrix} M_{x_{VT}} \\ M_{y_{VT}} \\ M_{z_{VT}} \end{pmatrix}^b + \begin{pmatrix} M_{x_{HT}} \\ M_{y_{HT}} \\ M_{z_{HT}} \end{pmatrix}^b\right] \tag{90}$$

$$\begin{aligned} A_{1c} &= -\theta_{1c} + \Theta_{MRc} \\ B_{1c} &= -\theta_{1s} + \Theta_{MRs} \end{aligned} \tag{91}$$

$$C_1 = -0.5.\sigma_{MR}.CL_{MR_\alpha}.\rho.\pi.R^2_{rot}.V^2_{MRref} \tag{92}$$

For a better response in the yaw channel, we introduced the expressions $\Theta_{TRp}.p$ and $\Theta_{TRr}.r$ in the tail rotor inflow, containing thus the two empirical coefficients Θ_{TRp} and Θ_{TRr} (as a function of the μ_x scheduling variable) and multiplied by p and r respectively, see Eq (50). The inclusion of the p and r independent variables, as regressors, was based upon engineering judgment, although systematic methods do exist when it comes down to independent variables selection, i.e. through the computation of partial correlation coefficients, and checking for the partial $F-$ statistics values, see Ref. 100. The estimation process, applied at P_k operating regimes, is similar to the one outlined for the previous four coefficients, only now we use the $\dot{r}$ acceleration equations from Eq (4).

From Eq (4) and Eq (8), we have

$$\mathbf{M}^b_{exclTR,G_{Fus}} = \begin{pmatrix} M_{exclTR_x,G_{Fus}} \\ M_{exclTR_y,G_{Fus}} \\ M_{exclTR_z,G_{Fus}} \end{pmatrix}^b = \mathbb{I}_{Fus}.\begin{pmatrix} \dot{p} \\ \dot{q} \\ \dot{r} \end{pmatrix}^b + \begin{pmatrix} p \\ q \\ r \end{pmatrix}^b \times \left[\mathbb{I}_{Fus}.\begin{pmatrix} p \\ q \\ r \end{pmatrix}^b\right] - \left[\begin{pmatrix} M_{x_{MR}} \\ M_{y_{MR}} \\ M_{z_{MR}} \end{pmatrix}^b + \begin{pmatrix} M_{x_F} \\ M_{y_F} \\ M_{z_F} \end{pmatrix}^b + \begin{pmatrix} M_{x_{VT}} \\ M_{y_{VT}} \\ M_{z_{VT}} \end{pmatrix}^b + \begin{pmatrix} M_{x_{HT}} \\ M_{y_{HT}} \\ M_{z_{HT}} \end{pmatrix}^b + \begin{pmatrix} -y_F.F_{Zaero,G_{Fus}} + z_F.F_{Yaero,G_{Fus}} \\ -z_F.F_{Xaero,G_{Fus}} + x_F.F_{Zaero,G_{Fus}} \\ -x_F.F_{Yaero,G_{Fus}} + y_F.F_{Xaero,G_{Fus}} \end{pmatrix}^b\right] \tag{93}$$

Now combining with Eq (51), we obtain the tail rotor thrust coefficient as

$$Y_{TR} = M_{exclTR_z,G_{Fus}}/(x_{TR}.\Gamma.\rho.\pi.\Omega^2_{TR}.R^4_{rot_{TR}})/2.K_{TR_{corr}} \tag{94}$$

From the tail rotor model we also have

$$\left(\lambda_{dw_F} + \Theta_{TRp}.p + \Theta_{TRr}.r\right).\sqrt{\mu^2_{TRxy} + (\lambda_{dw_F} + \Theta_{TRp}.p + \Theta_{TRr}.r - \mu_{TRz})^2} = f_{TR}(\Theta_{TRp}, \Theta_{TRr}) \simeq Y_{TR} \tag{95}$$

Here the Θ_{TRp} and Θ_{TRr} coefficients do not appear linearly in the model, hence they are derived through weighted Nonlinear Least Squares (NLS),[99] again in an equation-error identification framework, giving

$$(\Theta_{TRp}\ \Theta_{TRr})^T = (A^T.W.A)^{-1}.A^T.W.Y \tag{96}$$

With W the matrix weights, and the vector Y and matrix A given by

$$Y = Y_{TR} - f_{TR}(\Theta_{TRp}, \Theta_{TRr}) \tag{97}$$

$$A = \left[\frac{\partial f_{TR}(\Theta_{TRp}, \Theta_{TRr})}{\partial \Theta_{TRp}} \quad \frac{\partial f_{TR}(\Theta_{TRp}, \Theta_{TRr})}{\partial \Theta_{TRr}}\right] \tag{98}$$

In our case Eq (98) is easily derived analytically. Finally, since NLS is known to be sensitive to initial starting values, and can exhibit erratic divergence due to for example numerical corruption,[101] we initialize the NLS by solving an algebraic, nonlinear, constrained optimization problem, similar in nature to the one presented in Section VIII.C, only now with $J(\mathbf{V}) = |\dot{r}|$.

VIII.E. Validation

Finally, we give some brief comments on the modeling validation process. Here, the predominant question reads as follows:[83] is the model adequately accurate and robust for its purpose ? The answer goes along some well-known strategies.[3] The first one consists in supplying both the model and FLIGHTLAB with an input different from the one used during the estimation process (basically, a separate validation data set), and compare the model and FLIGHTLAB outputs afterwards.[86,100] The second one consists in examining the differences between the FLIGHTLAB and estimated outputs, i.e. the residuals, through a number of statistical residual analysis tools.[86,102,103] The advantage here is that a separate validation data set may not be required, although these tests may also be applied to such a data set. Finally, to mitigate the effect of reaching local minima during the estimation, since some of the estimation problems are non-convex, this estimation process may be repeated several times, for the same model structure, but under slightly varying initial conditions. However, in this paper, only preliminary findings are presented, primarily based upon results from the estimation process, whereas validation data analysis will be presented in future publications.

IX. Simulation Results

We implemented our model in a MATLAB® environment,[104] with the simulation plots given in Appendix C, where only visual comparisons are provided. Further, comparisons of the model results, based upon the estimation process, with an equivalent helicopter FLIGHTLAB model are briefly reviewed hereunder. The modeled helicopter UAV belongs to the R/C flybarless two-bladed main rotor class, which physical characteristics are documented in Appendix B. Additionally, for the FLIGHTLAB model, the following options have been selected

- Articulated rotor, and blade element model. Quasi-steady airloads, based on the Peters-He three-state inflow model, with no stall delay effects.
- Bailey tail rotor.
- Ideal engine.

IX.A. Trim Results

A trim condition is equivalent to an equilibrium point, also called an operating point of a nonlinear system, which can be thought of as a specific flight condition.[28] Further, trim settings are a prerequisite for stability analysis, vibration studies, and control systems synthesis. Indeed, any flight vehicle should be able to maintain equilibrium during steady flight conditions, this means that the resultant forces and moments on the vehicle are equal to zero.[105] For helicopters however, the concept of trim is more complicated than of fixed-wing aircrafts.[106] A helicopter has components that rotate with respect to each other and with respect to the air mass. Hence, periodic forces and moments enter the dynamic equations, and we cannot simply eliminate them by averaging.[106] Hence we implemented our own trim routine, structured as a constrained optimization problem.[50]

From figure 1 to figure 9, the roll and pitch angles, main rotor power, and the four control input trim values are plotted as a function of body linear velocities (u, v, w), with w positive down. We see that, for the roll and pitch angles, the maximum absolute deviations do not exceed the range of [1°- 2°] for the longitudinal velocity case, and are much lower for the lateral and vertical cases. Further, we can see that the main rotor power trim results are in good agreement with FLIGHTLAB, with a maximum deviation of about 7% observed during starboard flight. For the main rotor collective, the strongest discrepancy from FLIGHTLAB is observed in hover and does not exceed 0.25°, whereas the tail rotor input shows good agreement along the longitudinal, lateral, and downwards flight axes. We notice however that for vertical upwards flight, especially above the range [3 m/s - 4 m/s], notable differences for the tail rotor input with FLIGHTLAB (up to 20% at high upwards speed) start to appear. These may probably be explained by distinct implementations of the tail rotor induced flow. Finally, the longitudinal and lateral control input exhibit very good agreement with FLIGHTLAB, along all three axes.

IX.B. Dynamic Results

For the validation of a model dynamic responses, we may consider two approaches. The first one consists in obtaining linearized models, for several P_m operating regimes, which describe the small perturbation motion about a trimmed equilibrium position. The validation is then carried out by comparing the frequency response predicted by the linearized models with those obtained from FLIGHTLAB.[92] The second approach consists in comparing the time histories of the models with those obtained from FLIGHTLAB. In this paper, we provide visual comparisons of time histories data with FLIGHTLAB for roll/pitch/yaw angles (ϕ, θ, ψ), linear velocities (u, v, w), and rotational velocities (p, q, r).

The tests are set to evaluate the open-loop response, at a constant main rotor RPM, of this highly unstable and nonlinear model. First, the rotor is set in a steady-state condition during a time period of 0.5 s. Then, for the following 3 s, we simultaneously apply on the four input channels, a sinusoid of 1° in amplitude, at a frequency of 2 Hz[u]. Again and as mentioned in Section VIII.E we use here, as control input signal, one of the signals used during the estimation process.

The first test is run from a hover trim condition, see figure 10, the second test is carried out to evaluate the medium speed characteristics at $u = 5$ m/s, see figure 11, whereas the third trial is run to check the high speed flight at $u = 10$ m/s, see figure 12. Here it can be seen that all states exhibit a good to very good match with FLIGHTLAB, except for the yaw channel (ψ, r) and sidewards channel v. For the first one, it shows for example a 10° heading angle mismatch after 3 s in hover. However, this discrepancy tends to decrease as the helicopter forward velocity increases, due to increased speed stability in the yaw channel. For the lateral velocity, we see an opposite effect, the deviations from FLIGHTLAB increase as the forward velocity increases. At the cost of additional model complexity, we believe that most of the here above observed differences, although being relatively small, could potentially be improved by inserting an additional empirical correction factor[v], which role would be to (better) approximate the main rotor sideforce.

[u] Corresponding to the maximum anticipated closed-loop system bandwidth for autonomous flight.

[v] However, a model should not be more flexible then necessary. To overcome any high variance of the estimated parameters, it is important to restrict the number of empirical coefficients.

X. Conclusion

The main objective of this paper is to develop and study a helicopter UAV modeling framework, that we believe may be useful, when solving for optimal trajectories through numerical optimizations methods, such as constrained nonlinear optimal control. The idea here consists in combining the grey-box modeling paradigm with the multiple-model approach, where we partition the system's full operating range in several operating regimes. In principle, this obtained framework generates a high modeling fidelity, and supports incremental modeling, simple model maintenance to some extent, and allows for substantial computational speed improvement.

Now regarding our model accuracy, and when compared with an equivalent FLIGHTLAB model, initial findings suggest that a promising level of model quality has been achieved. In order to emulate the experimental data needed for the estimation process, the current framework makes extensive use of FLIGHTLAB, first by using some data which are generally not provided by a classical UAV sensors suite, and second by assuming that all provided measurements are noise-free. However, the aim of our future work is to relax these constraints, by setting-up a modeling and identification framework, based upon measured data, which shall be able to estimate both the empirical coefficients of the grey-box model, together with system's physical parameters, such as helicopter inertia, flap hinge stiffness, etc.

Appendix A: Nomenclature

- Frames

F_I	Geocentric inertial frame
F_E	Normal earth fixed frame
F_o	Vehicle carried normal earth frame
F_b	Body (vehicle) frame
F_a	Aerodynamic (air path) frame
F_k	Kinematic (flight path) frame
F_{HB}	Hub-Body frame
F_{HB}	Hub-Body frame
F_{HBw}	Hub-Body wind-axis frame
F_{TR}	Tail-Rotor frame

- Frame origins

A	Origin of frame F_I, earth center
O	Origin of frames F_E and F_o, an earth surface point
G	Origin of frames F_b, F_a and F_k, aircraft center of mass

- Angles between frames

ψ	Azimuth angle (yaw angle, heading)
θ	Inclination angle (pitch angle, or elevation)
ϕ	Bank angle (roll angle)

- Position

x_N, x_E, x_Z	Coordinates of CG position vector in F_E frame
x_H, y_H, z_H	Coordinates of Hub position wrt vehicle CG in F_b frame

- Altitude

$h_H = -x_Z - z_H$	Hub position above ground

- Linear velocities are denoted $\mathbf{V}$ and their components u, v, w

$\mathbf{V}_{k,G}$	Kinematic velocity of the vehicle center of mass
$\mathbf{V}_{a,G}$	Aerodynamic velocity of the vehicle center of mass
$u_k^o = V_N$	x component of $\mathbf{V}_{k,G}$ on F_o, V_N North velocity
$v_k^o = V_E$	y component of $\mathbf{V}_{k,G}$ on F_o, V_E East velocity
$w_k^o = V_Z$	z component of $\mathbf{V}_{k,G}$ on F_o, V_Z Vertical velocity
$u_k^b = u$	x component of $\mathbf{V}_{k,G}$ on body frame F_b
$v_k^b = v$	y component of $\mathbf{V}_{k,G}$ on body frame F_b
$w_k^b = w$	z component of $\mathbf{V}_{k,G}$ on body frame F_b

- Angular velocities are denoted $\mathbf{\Omega}$ and their components p, q, r

$\mathbf{\Omega}_k = \mathbf{\Omega}_{bE}$	Kinematic angular velocity of the vehicle (b) relative to the earth (E)
$p_k^b = p$	Roll velocity (roll rate) of the vehicle relative to the earth (frame F_E)
$q_k^b = q$	Pitch velocity (pitch rate) of the vehicle relative to the earth
$r_k^b = r$	Yaw velocity (yaw rate) of the vehicle relative to the earth

- Wind

$\mathbf{V}_w$	Wind linear velocity in F_E, of an atmospheric particle which could have been located at the vehicle center of mass
u_w	Wind x-velocity in F_E
v_w	Wind y-velocity in F_E
w_w	Wind z-velocity in F_E
p_w	Wind roll-velocity in F_E
q_w	Wind pitch-velocity in F_E
r_w	Wind yaw-velocity in F_E
Ψ_w	Wind azimuthal angular position
ρ	Air density

- Mass

m	Vehicle total mass

- Main Rotor (MR) properties

Γ	Direction of rotation, $CCW : \Gamma = 1 \quad CW : \Gamma = -1$
N_b	Number of blades
M_{bl}	Blade 0th mass moment (blade mass from flap hinge)
$C_0 = M_{bl} \cdot y_{G_{bl}}$	Blade 1st mass moment
I_β	Blade 2nd mass moment (inertia about flap hinge)
I_b	Blade 2nd mass moment (inertia about rotor shaft)
R_{rot}	Rotor radius measured from hub center
R_{bl}	Blade radius measured from flap hinge
Δ_e	Distance between hub and flap hinge
c_{bl}	Blade chord
$y_{G_{bl}}$	Blade CG radial position from flap hinge
$\sigma_{MR} = \frac{N_b . c_{bl}}{\pi . R_{rot}}$	Solidity
B	Tip loss factor, expressed as percentage of blade length R_{bl} no lift is generated outboard of position $B.R_{bl}$
$\gamma = \frac{\rho . c_{bl} . CL_{MR\alpha} . R_{bl}^4}{I_\beta}$	Blade Lock number
λ_m	Momentum theory induced flow due to rotor thrust (TPP)
λ_h	Rotor induced inflow in hover $\lambda_h = \sqrt{\frac{C_{T_{MR}}}{2}} = v_h / V_{MRref}$
μ	Advance ratio
μ_x	Non-dimensional forward flight air velocity
μ_y	Non-dimensional sidewards flight air velocity
$\mu_{xy} = \sqrt{\mu_x^2 + \mu_y^2}$	Non-dimensional in-plane (rotor disk) air velocity
μ_z	Non-dimensional vertical flight air velocity (normal to the TPP)
K_{S_β}	Hub spring restraint coefficient (due to flap)
$\bar{\mu} = \frac{\mu}{\lambda_h}$	Normalizing advance ratio
$\bar{\lambda} = \frac{\lambda_m + \mu_z}{\lambda_h}$	Normalizing total inflow
G_{eff}	Ground effect corrective factor
$\epsilon = \frac{\Delta_e}{R_{rot}}$	Normalized flap hinge offset

- Main Rotor (MR) properties (Cont'd)

Θ_{MRc}	Trim bias on lateral cyclic pitch in TPP expressions
Θ_{MRs}	Trim bias on longitudinal cyclic pitch in TPP expressions
Θ_{MRp1}	Form factor on roll rate in TPP expressions
Θ_{MRp2}	Form factor on roll rate in TPP expressions
Θ_{MRq1}	Form factor on pitch rate in TPP expressions
Θ_{MRq2}	Form factor on pitch rate in TPP expressions
Θ_{MRvrs}	Form factor on rotor inflow in the VRS
Θ_{MRpwr}	Form factor on rotor power

- MR position vector components

x_H, y_H, z_H	Position of Hub center wrt vehicle CG G

- MR angles

ψ_{bl}	Azimuthal angular position of blade
β_0	Rotor TPP coning angle
β_{1c}	Longitudinal rotor TPP tilt (positive forward)
β_{1s}	Lateral rotor TPP tilt (positive towards retreating side)
θ_{bl}	Blade pitch outboard of flap hinge (feathering) angle
ψ_{PA}	Swashplate phase angle
θ_0	Blade root collective pitch
θ_{1c}	Lateral cyclic pitch
θ_{1s}	Longitudinal cyclic pitch
β_{MR}	Sideslip angle

$$\begin{aligned}\beta_{bl} &\simeq \beta_0 + \beta_{1c}\cos\psi_{bl} + \beta_{1s}\sin\psi_{bl}\\ \theta_{bl} &= \theta_0 + \theta_{1c}\cos(\psi_{bl}+\psi_{PA}) + \theta_{1s}\sin(\psi_{bl}+\psi_{PA})\end{aligned}$$

- MR angular velocities

$\Omega_{MR_{100\%}}$	Nominal (100%) angular velocity
Ω_{MR}	Instantaneous angular velocity

- MR linear velocities

v_{i_o}	Rotor uniform induced velocity, normal to the TPP and positive when oriented downwards
v_h	Rotor induced velocity in hover $v_h = \sqrt{\frac{m.g}{2.\rho.\pi.R_{rot}^2}}$
V_{MRref}	Reference velocity $V_{MRref} = \Omega_{MR}.R_{rot}$

- MR forces/moments

$F_{x_{MR}}$	x-force
$F_{y_{MR}}$	y-force
$F_{z_{MR}}$	z-force
$M_{x_{MR}}$	Total roll moment
$M_{y_{MR}}$	Total pitch moment
$M_{z_{MR}}$	Total yaw moment
$L_{(MR,inertial)}$	Roll moment due to inertia loads
$M_{(MR,inertial)}$	Pitch moment due to inertia loads
$L_{(MR,flap)}$	Roll moment due to hub spring restraint (flap)
$M_{(MR,flap)}$	Pitch moment due to hub spring restraint (flap)
$N_{(MR,aero)} = Q_{MR}$	Yaw moment due to aerodynamic loads
P_{MR}	Power

- MR aerodynamic and force/moments coefficients

C_{HMR}	Drag coefficient
C_{YMR}	Side-force coefficient
C_{TMR}	Thrust coefficient
CL_{MR_α}	Blade section lift curve slope
CL_{MR}	Lift coefficient
CD_{MR}	Mean drag coefficient (profile drag)

- Tail Rotor (TR) properties

$N_{b_{TR}}$	Number of blades
$R_{rot_{TR}}$	Rotor radius measured from shaft
$\frac{\partial \beta_{0_{TR}}}{\partial T_{TR}}$	Partial coning angle wrt thrust
$\tan \delta_{3_{TR}}$	Tangent of hinge skew angle for pitch-flap coupling
c_{TR}	Blade chord
$\sigma_{TR} = \frac{N_{b_{TR}}.c_{TR}}{\pi.R_{rot_{TR}}}$	Solidity
μ_{TRx}	x-component of advance ratio
μ_{TRy}	y-component of advance ratio
	$\mu^2_{TRxy} = \mu^2_{TRx} + \mu^2_{TRy}$
μ_{TRz}	z-component of advance ratio
λ_{TR}	Total inflow
λ_{dw}	Inflow
$t_1 \quad t_2$	Bailey coefficients
CL_{TR_α}	Blade section lift curve slope
CD_{TR}	Mean drag coefficient (profile drag)
B_{TR}	Tip loss factor, expressed as percentage of blade length
Θ_{TRp}	Form factor on roll rate in inflow expression
Θ_{TRr}	Form factor on yaw rate in inflow expression
$K_{TR_{corr}}$	Correction factor

- TR position vector components

x_{TR}, y_{TR}, z_{TR}	Position wrt vehicle CG (in F_{HB} frame)

- TR angles

$\beta_{0_{TR}}$	Coning angle
θ_{TR}	Blade pitch angle
$\theta_{0_{TR}}$	Blade root collective pitch
$\theta_{bias_{TR}}$	Preset collective pitch bias

- TR angular velocities

$\Omega_{TR_{100\%}}$	Nominal (100%) angular velocity
Ω_{TR}	Instantaneous angular velocity

- TR linear velocities

$\mathbf{V}_{a,TR}$	Aerodynamic velocity of the TR hub
V_{TRref}	Reference velocity
	$V_{TRref} = \Omega_{TR}.R_{rot_{TR}}$

- TR forces/moments
  - T_{TR} Thrust
  - $F_{x_{TR}}$ x-force
  - $F_{y_{TR}}$ y-force
  - $F_{z_{TR}}$ z-force
  - $M_{x_{TR}}$ Total roll moment
  - $M_{y_{TR}}$ Total pitch moment
  - $M_{z_{TR}}$ Total yaw moment
- Fuselage (Fus) properties
  - S_{ref_F} Reference area
  - L_{ref_F} Reference length
- Fuselage angles
  - α_F Angle of attack
  - β_F Sideslip angle
- Fuselage position vector components
  - x_F, y_F, z_F Position of fuselage CG wrt
- Fuselage forces/moments
  - F_{x_F} x-force
  - F_{y_F} y-force
  - F_{z_F} z-force
  - M_{x_F} Total roll moment
  - M_{y_F} Total pitch moment
  - M_{z_F} Total yaw moment
- Horizontal/Vertical Tails (HTVT) properties
  - $S_{ref_{HT}}$ HT Reference area
  - $L_{ref_{HT}}$ HT Reference length
  - $S_{ref_{VT}}$ VT Reference area
  - $L_{ref_{VT}}$ VT Reference length
- Horizontal/Vertical Tails (HTVT) angles
  - α_{HT} HT angle of attack
  - β_{HT} HT sideslip angle
  - α_{VT} VT angle of attack
  - β_{VT} VT sideslip angle
- Horizontal/Vertical Tails (HTVT) position vector components
  - x_{HT}, y_{HT}, z_{HT} Position of horizontal tail aerodynamic center
  - x_{VT}, y_{VT}, z_{VT} Position of vertical tail aerodynamic center

- Horizontal/Vertical Tails (HTVT) forces/moments

$F_{x_{HT}}$	HT x-force
$F_{y_{HT}}$	HT y-force
$F_{z_{HT}}$	HT z-force
$F_{x_{VT}}$	VT x-force
$F_{y_{VT}}$	VT y-force
$F_{z_{VT}}$	VT z-force
$M_{x_{HT}}$	Total HT roll moment
$M_{y_{HT}}$	Total HT pitch moment
$M_{z_{HT}}$	Total HT yaw moment
$M_{x_{VT}}$	Total VT roll moment
$M_{y_{VT}}$	Total VT pitch moment
$M_{z_{VT}}$	Total VT yaw moment

Appendix B: Physical Parameters

	Name	Parameter	Value	Unit
Environment	Air density	ρ	1.2367	kg/m^3
	Static temperature	T	273.15 + 15	K
	Specific heat ratio (air)	γ	1.4	
	Gas constant (air)	R	287.05	$J/kg.K$
	Gravity constant	g	9.812	m/s^2
Vehicle	Total mass	m	8.35	kg
	Inertia moment wrt x_b	A	0.338	$kg.m^2$
	Inertia moment wrt y_b	B	1.052	$kg.m^2$
	Inertia moment wrt z_b	C	1.268	$kg.m^2$
	Inertia product wrt x_b	D	0.001	$kg.m^2$
	Inertia product wrt y_b	E	0.002	$kg.m^2$
	Inertia product wrt z_b	F	0	$kg.m^2$
Main Rotor	Direction of rotation	Γ	CW (-1)	
	Number of blades	N_b	2	
	Nominal angular velocity	$\Omega_{MR_{100\%}}$	151.84	rad/s
	Rotor radius from hub	R_{rot}	0.933	m
	Blade mass	M_{bl}	0.218	kg
	Spring restraint coef. due to flap	K_{S_β}	271.1635	$N.m/rad$
	Distance between hub and flap hinge	Δ_e	0.094	m
Tail Rotor	Number of blades	2		
	Nominal angular velocity	$\Omega_{TR_{100\%}}$	709.11	rad/s
	Rotor radius from rotor hub	$R_{rot_{TR}}$	0.17	m
Actuators	MR collective	θ_0	[-2.8,13.7].π/180	rad
	TR collective	θ_{TR}	[-27,32.8].π/180	rad
	MR lateral cyclic	θ_{1c}	[-6.8,6].π/180	rad
	MR longitudinal cyclic	θ_{1s}	[-7.8,5].π/180	rad
	MR collective rate	$\dot{\theta}_0$	[-52,52].π/180	rad/s
	TR collective rate	$\dot{\theta}_{TR}$	[-120,120].π/180	rad/s
	MR lateral cyclic rate	$\dot{\theta}_{1c}$	[-56,56].π/180	rad/s
	MR longitudinal cyclic rate	$\dot{\theta}_{1s}$	[-56,56].π/180	rad/s

Appendix C: Simulation Results

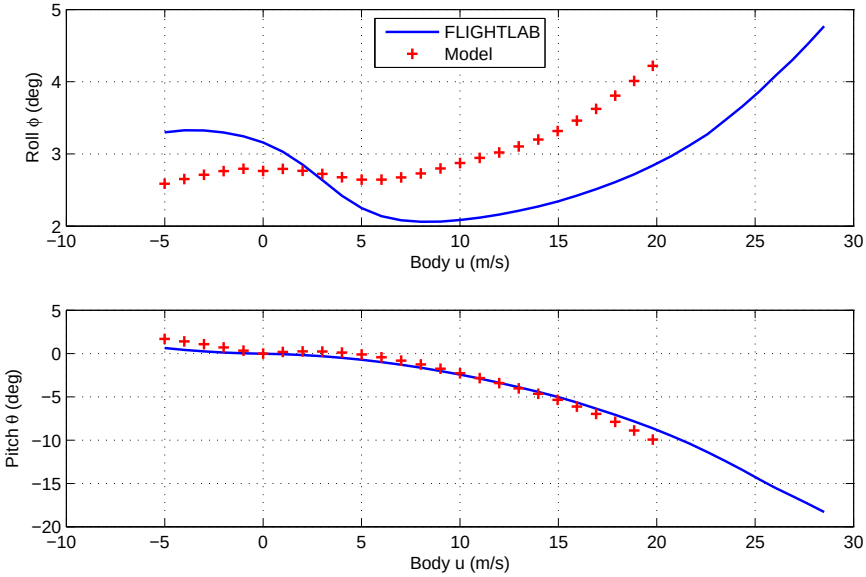

Figure 1. Trim: roll/pitch angles as a function of body longitudinal velocity u

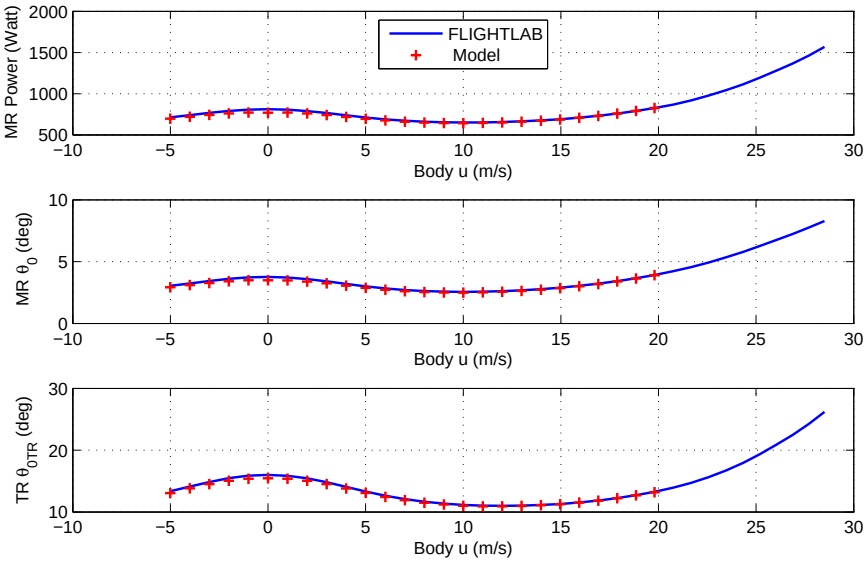

Figure 2. Trim: MR power and MR/TR collective pitch angles as a function of body longitudinal velocity u

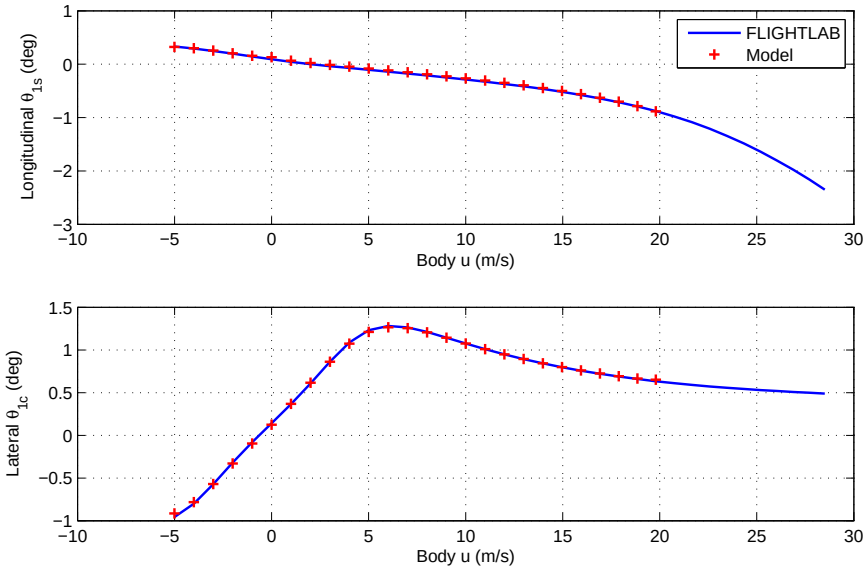

Figure 3. Trim: MR longitudinal and lateral cyclic pitch angles as a function of body longitudinal velocity u

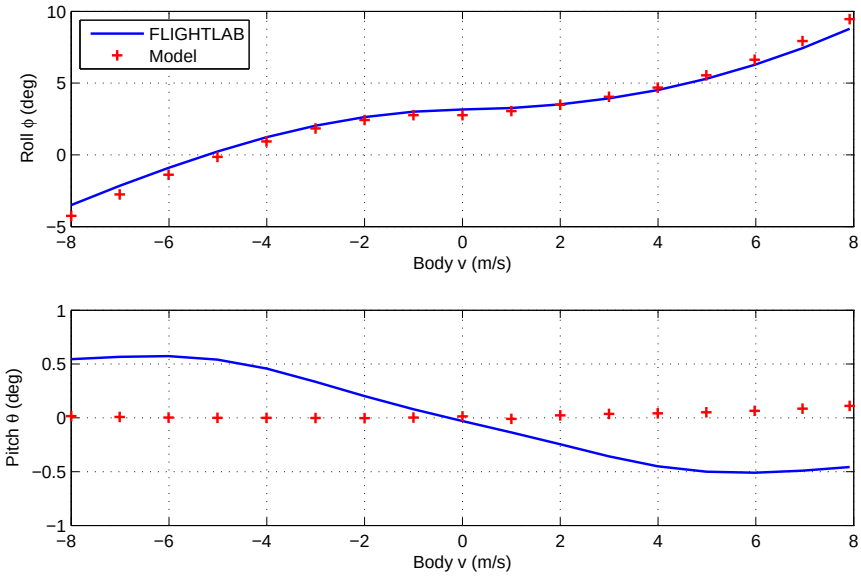

Figure 4. Trim: roll and pitch angles as a function of body lateral velocity v

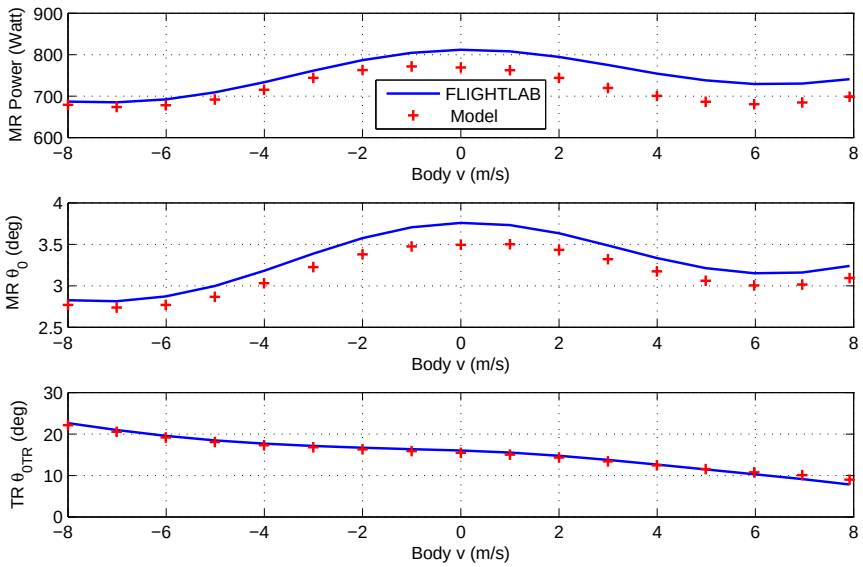

Figure 5. Trim: MR power and MR/TR collective pitch angles as a function of body lateral velocity v

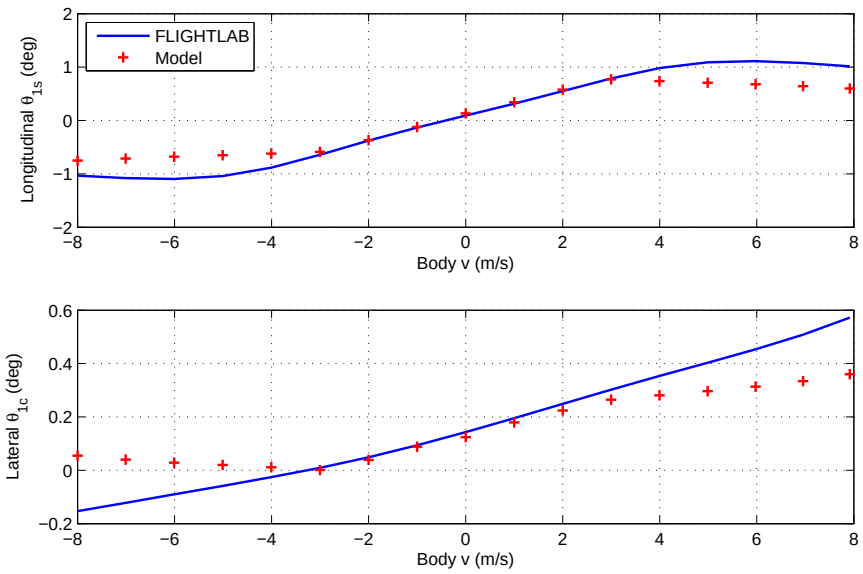

Figure 6. Trim: MR longitudinal and lateral cyclic pitch angles as a function of body lateral velocity v

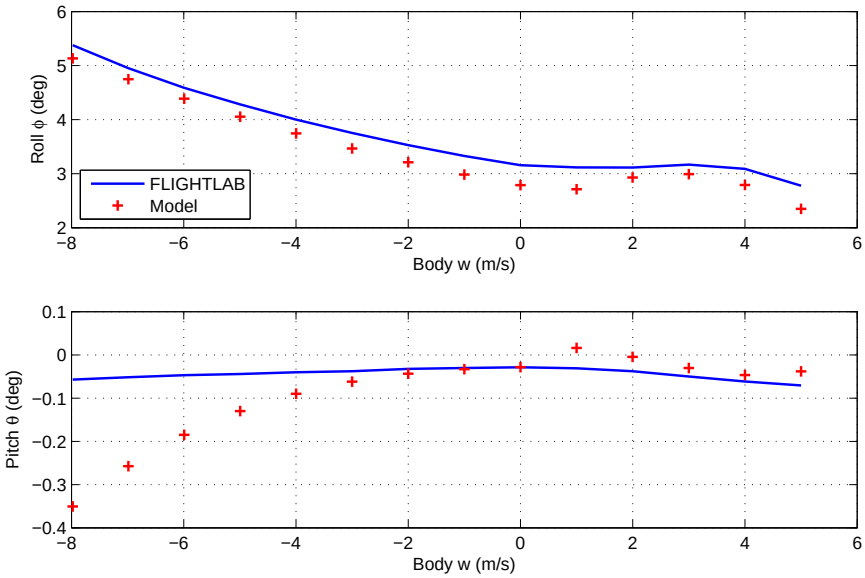

Figure 7. Trim: roll and pitch angles as a function of body vertical velocity w

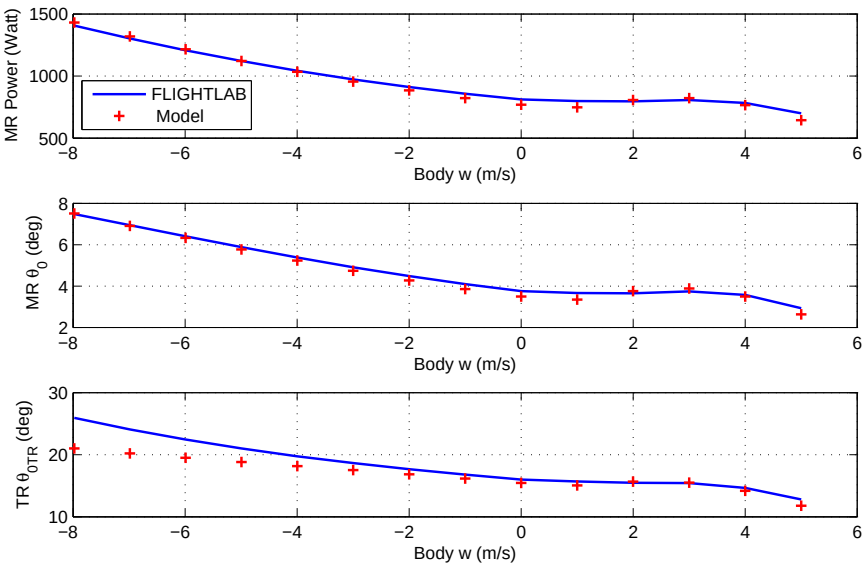

Figure 8. Trim: MR power and MR/TR collective pitch angles as a function of body vertical velocity w

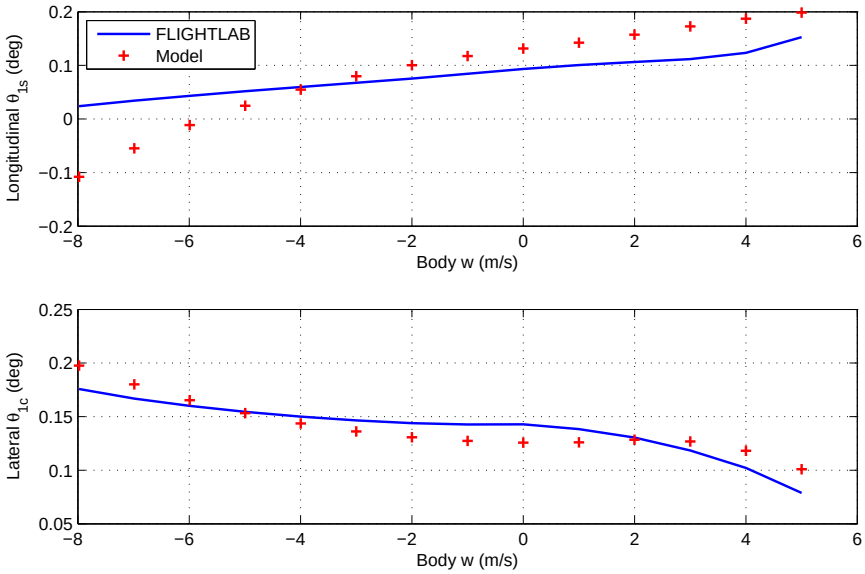

Figure 9. Trim: MR longitudinal and lateral cyclic pitch angles as a function of body vertical velocity w

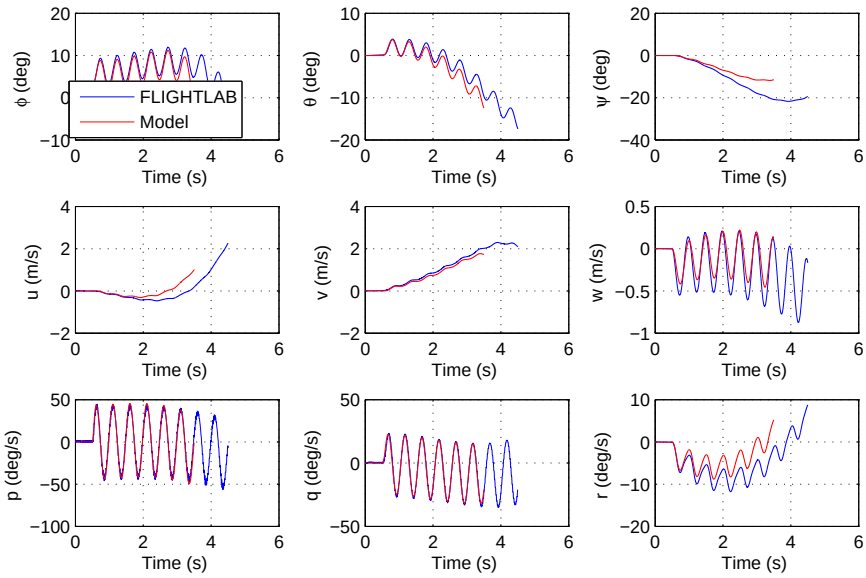

Figure 10. Vehicle response to sinusoidal inputs (at hover)

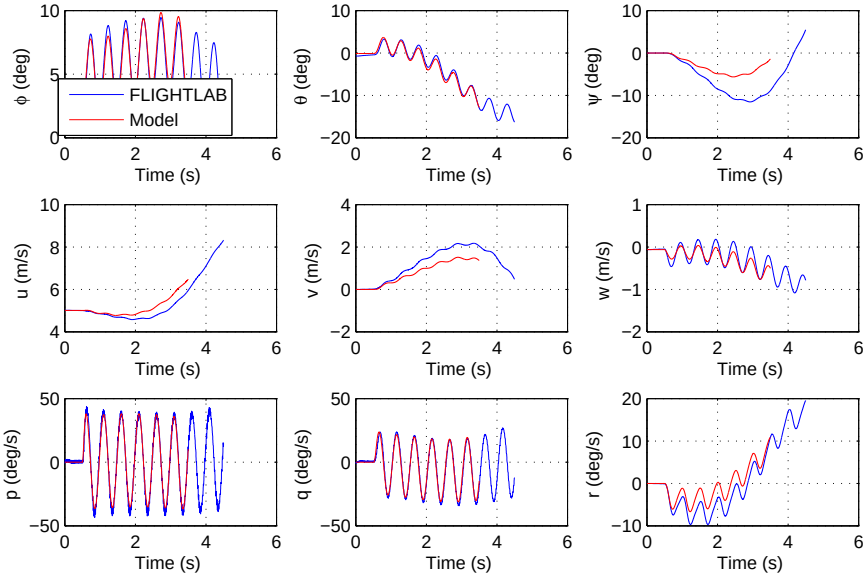

Figure 11. Vehicle motion: response to sinusoidal inputs (at $u = 5$ m/s)

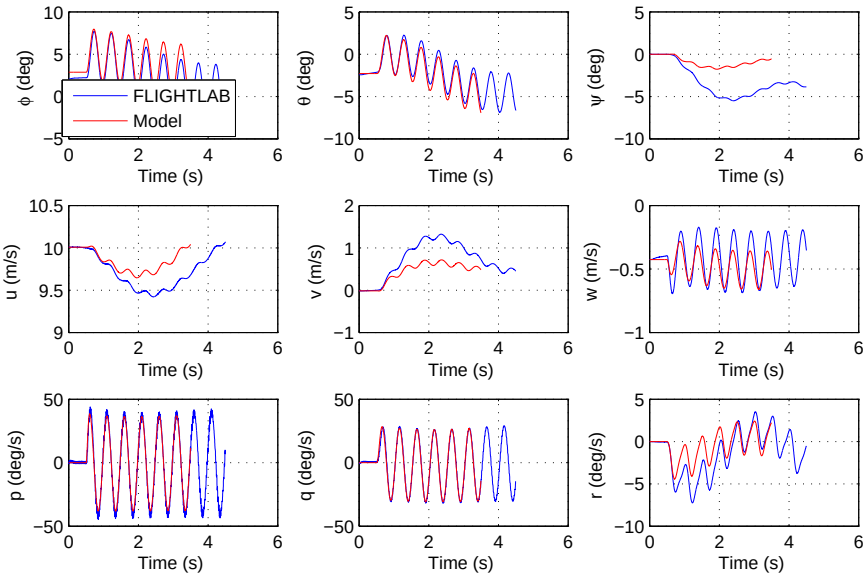

Figure 12. Vehicle response to sinusoidal inputs (at $u = 10$ m/s)

References

[1]DoD, "Unmanned Aircraft Systems (UAS) Roadmap 2005-2030," Tech. rep., U.S.A. DoD, 2005.

[2]Johansen, T. A., *Operating Regime Based Process Modeling and Identification*, Ph.D. thesis, Norwegian Institute of Technology, 1994.

[3]Angelis, G. Z., *System Analysis, Modelling and Control with Polytopic Linear Models*, Ph.D. thesis, Eindhoven University of Technology, 2001.

[4]Chalmers, A. F., *What is this Thing Called Science ?*, Open University Press, 1982.

[5]Romijn, R., Ozkan, L., Weiland, S., Ludlage, J., and Marquardt, W., "A Grey-Box Modeling Approach For The Reduction Of Nonlinear Systems," *8th International IFAC Symposium on Dynamics and Control of Process Systems*, 2007.

[6]Taamallah, S., "Optimal Autorotation With Obstacle Avoidance For A Small-Scale Flybarless Helicopter UAV," *AIAA Guidance, Navigation and Control Conference*, 2012.

[7]Taamallah, S., Bombois, X., and den Hof, P. V., "Optimal Control For Power-Off Landing Of A Small-Scale Helicopter A Pseudospectral Approach," *American Control Conference*, 2012.

[8]Pallett, T. J. and Ahmad, S., "Real-Time Helicopter Flight Control: Modelling and Control by Linearization and Neural Networks," Tech. Rep. TR-EE 91-35, Purdue University School of Electrical Engineering, 1991.

[9]Morris, J. C., van Nieuwstadt, M., and Bendotti, P., "Identification and Control of a Model Helicopter in Hover," *American Control Conference*, 1994.

[10]Weilenmann, M. F. and Geering, H. P., "Test Bench for Rotorcraft Hover Control," *AIAA Journal of Guidance, Control, and Dynamics*, Vol. 17, No. 4, 1994, pp. 729–736.

[11]Bendotti, P. and Morris, J. C., "Robust Hover Control for a Model Helicopter," *American Control Conference*, 1995.

[12]Conway, A., *Autonomous Control of an Unstable Helicopter Using Carrier Phase GPS Only*, Ph.D. thesis, Stanford University, 1995.

[13]Johnson, E. N. and DeBitetto, P. A., "Modeling and Simulation for Small Autonomous Helicopter Development," *AIAA Modeling and Simulation Technologies Conference*, 1997.

[14]Grady, N. B., Frye, M. T., and Qian, C., "The Instrumentation and Flight Testing of a Rotorcraft Vehicle for Undergraduate Flight Control Research," *AIAA Modeling and Simulation Technologies Conference and Exhibit*, 2006.

[15]Cai, G., Chen, B. M., Peng, K., Dong, M., and Lee, T. H., "Modeling and control system design for a UAV helicopter," *Proceedings of the 14th Mediterranean Conference on Control and Automation*, 2006.

[16]Velez, C. M., Agudelo, A., and Alvarez, J., "Modeling, Simulation and Rapid Prototyping of an Unmanned Mini-Helicopter," *AIAA Modeling and Simulation Technologies Conference and Exhibit*, 2006.

[17]Zhao, L. and Murthy, V. R., "Optimal Controller for an Autonomous Helicopter in Hovering and Forward Flight," *47th AIAA Aerospace Sciences Meeting*, 2009.

[18]Khaligh, S. P., Fahimi, F., and Saffarian, M., "Comprehensive Aerodynamic Modeling of a Small Autonomous Helicopter Rotor at All Flight Regimes," *AIAA Modeling and Simulation Technologies Conference*, 2009.

[19]Furuta, K., Ohyama, Y., and Yamano, O., "Dynamics of RC Helicopter And Control," *Mathematics and Computers in Simulation*, Vol. 26, 1984, pp. 148–159.

[20]Kim, S. K. and Tilbury, T. M., "Mathematical Modeling and Experimental Identification of a Model Helicopter," *AIAA Modeling and Simulation Technologies Conference*, 1998.

[21]Munzinger, C., "Development of a Real-Time Flight Simulator for an Experimental Model Helicopter," Tech. rep., Master Thesis, Georgia Institute of Technology, 1998.

[22]Shim, D. H., *Hierarchical Control System Synthesis for Rotorcraft-based Unmanned Aerial Vehicles*, Ph.D. thesis, University of California at Berkeley, 2000.

[23]Civita, M. L., *Integrated Modeling and Robust Control for Full-Envelope Flight of Robotic Helicopters*, Ph.D. thesis, Carnegie Mellon University, 2002.

[24]Cunha, R. and Silvestre, C., "Dynamic Modeling and Stability Analysis of Model-Scale helicopters with Bell-Hiller Stabilzing Bar," *AIAA Guidance, Navigation, and Control Conference*, 2003.

[25]Tanner, O., *Modeling, Identification, and Control of Autonomous Helicopters*, Ph.D. thesis, ETH Zurich, 2003.

[26]de Jong, A., "Helicopter UAV Control Using Classical Control," Tech. rep., Master Thesis, Delft University of Technology, 2004.

[27]Sudiyanto, T., Budiyono, A., and Sutarto, H. Y., "Hardware In-the-Loop Simulation for Control System Designs of Model Helicopter," *Aerospace Indonesia Meeting, Bandung*, 2005.

[28]Hald, U. B., Hesselbaek, M. V., and Siegumfeldt, M., "Nonlinear Modeling and Optimal Control of a Miniature Autonomous Helicopter," Tech. rep., Master Thesis, Aalborg University, 2006.

[29]Bhandari, S. and Colgren, R., "6-DoF Dynamic Model for a Raptor 50 UAV Helicopter Including Stabilizer Bar Dynamics," *AIAA Modeling and Simulation Technologies Conference*, 2006.

[30]Czyba, R., "Modelling of Unmanned Model-Scale Helicopter Dynamics for Needs of the Simulator," *11th IFAC Symposium on Large Scale Complex Systems Theory and Applications*, 2007.

[31]Cai, G., Chen, B. M., Lee, T. H., and Lum, K. Y., "Comprehensive Nonlinear Modeling of an Unmanned-Aerial-Vehicle Helicopter," *AIAA Guidance, Navigation and Control Conference*, 2008.

[32]Andersen, T. L., Lauritzen, D. F., Madsen, J. T., Sorensen, M. M., and Mertz, B. A., "Autonomous Inverted Hover of a Small Scale Helicopter," Tech. rep., Aalborg University, 2008.

[33]Bagnell, J. and Schneider, J., "Autonomous Helicopter Control Using Reinforcement Learning Policy Search Methods," *International Conference on Robotics and Automation*, 2001.

[34]Buskey, G., Roberts, O., Corke, P., Ridley, P., and Wyeth, G., *Sensing and Control for a Small-Size Helicopter. in Experimental Robotics VIII, pp. 476-486*, Springer, Berlin/Heidelberg, 2003.

[35]Ng, A. Y., Kim, H. J., Jordan, M., and Sastry, S., "Autonomous Helicopter Flight via Reinforcement Learning," *Neural Information Processing Systems (NIPS)*, 2004.

[36]Engel, J. M., "Reinforcement Learning Applied to UAV Helicopter Control," Tech. rep., Master Thesis, Delft University of Technology, 2005.

[37]Amidi, O., *An Autonomous Vision-Guided Helicopter*, Ph.D. thesis, Carnegie Mellon University, 1996.

[38]Shakernia, O., Sharp, C. S., Vidal, R., Shim, D. H., Ma, Y., and Sastry, S., "Multiple View Motion Estimation and Control for Landing an Unmanned Aerial Vehicle," *International Conference on Robotics and Automation*, 2002.

[39]Roberts, J. M., Corke, P. I., and Buskey, G., "Low-Cost Flight Control System for a Small Autonomous Helicopter," *Australian Conference on Robotics and Automation*, 2002.

[40]Saripalli, S., Montgomery, J. F., and Sukhatme, G. S., "Visually-Guided Landing of an Autonomous Aerial Vehicle," *IEEE Transactions on Robotics and Automation*, Vol. 19, No. 3, 2003, pp. 371–381.

[41]Saripalli, S. and Sukhatme, G., "Landing on a Moving Target using an Autonomous Helicopter," *International Conference on Field and Service Robotics*, 2003.

[42]Barabanov, A. E., Vazhinsky, N. Y., and Romaev, D. V., "Full Autopilot for Small Electrical Helicopter," *33th European Rotorcraft Forum*, 2007.

[43]Gavrilets, V., Mettler, B., and Feron, E., "Nonlinear Model for a Small-Size Acrobatic Helicopter," *AIAA Guidance, Navigation and Control Conference*, 2001.

[44]Mettler, B., *Identification Modelling and Characteristics of Miniature Rotorcraft*, Kluwer Academic Publishers, Norwell Mass, USA, 2003.

[45]Marconi, L. and R.Naldi, "Robust NonLinear Control for a Miniature Helicopter for Aerobatic Maneuvers," *32nd European Rotorcraft Forum*, 2006.

[46]Ng, A. Y., Coates, A., Diel, M., Ganapathi, V., Schulte, J., Tse, B., Berger, E., and Liang, E., "Autonomous Inverted Helicopter Flight via Reinforcement Learning," *International Symposium on Experimental Robotics*, 2004.

[47]Abbeel, P., Coates, A., Quigley, M., and Ng, A. Y., "An application of reinforcement learning to aerobatic helicopter flight," *NIPS 19*, 2007.

[48]Abbeel, P., Coates, A., Hunter, T., and Ng, A. Y., "Autonomous Autorotation of an RC Helicopter," *11th International Symposium on Experimental Robotics (ISER)*, 2008.

[49]Taamallah, S., "Small-Scale Helicopter Blade Flap-Lag Equations of Motion For A Flybarless Pitch-Lag-Flap Main Rotor," *AIAA Modeling and Simulation Technologies Conference*, 2011.

[50]Taamallah, S., "Flight Dynamics Modeling For A Small-Scale Flybarless Helicopter UAV," *AIAA Atmospheric Flight Mechanics Conference*, 2011.

[51]Taamallah, S., "A Flight Dynamics Helicopter UAV Model For A Single Pitch-Lag-Flap Main Rotor: Modeling & Simulations," Tech. Rep. NLR-TP-2010-286-PT-1, NLR, 2011.

[52]Seckel, E. and Curtiss, H. C., "Aerodynamic Characteristics of Helicopter Rotors," Tech. Rep. No. 659, Department of Aerospace and Mechanical Engineering, Princeton University, 1962.

[53]Chen, R. T. N., "A Simplified Rotor System Mathematical Model for Piloted Flight Dynamics Simulation," Tech. Rep. NTM 78575, NASA Ames Research Center, 1979.

[54]Chen, R. T. N., "Effects of Primary Rotor Parameters on Flapping Dynamics," Tech. Rep. NTP 1431, NASA Ames Research Center, 1980.

[55]Boiffier, J. L., *The Dynamics of Flight The Equations*, John Wiley & Sons, Chichester, England, 1998.

[56]Misra, P. and Enge, P., *Global Positioning System: Signals, Measurements and Performance, Second Edition*, Ganga-Jamuna Press, Lincoln MA, USA, 2006.

[57]Padfield, G. D., *Helicopter Flight Dynamics*, Blackwell Science Ltd, Oxford, UK, 1996.

[58]Gessow, A. and Myers, G. C., *Aerodynamics of the Helicopter*, College Park Pr, 1999.

[59]Johnson, W., *Helicopter Theory*, Dover Publications Inc., NY, USA, 1994.

[60]Bramwell, A. R. S., *Bramwell's Helicopter Dynamics, Second Edition*, AIAA Inc., Reston VA, USA, 2001.

[61]Shevell, R. S., *Fundamentals of Flight*, Prentice Hall, Upper Saddle River NJ, 1989.

[62]Anderson, J. D., *Fundamentals of Aerodynamics. Third Ed.*, McGraw-Hill Higher Education, NY, 2001.

[63]Prouty, R. W., *Helicopter Performance, Stability, and Control*, Krieger Publishing Company, Malabar, Florida USA, 1995.

[64]Houck, J. A., Moore, F. L., Howlett, J. J., Pollock, K. S., and Browne, M. M., "Rotor Systems research Aircraft Simulation Mathematical Model," Tech. Rep. NTM 78629, NASA Langley Research Center, 1977.

[65]Pitt, D. M. and Peters, D. A., "Theoretical Prediction of Dynamic-Inflow Derivatives," *Vertica*, Vol. 5, 1981, pp. 21–34.

[66]Peters, D. A. and HaQuang, N., "Technical Notes - Dynamic Inflow for Practical Applications," *Journal of the American Helicopter Society*, 1988, pp. 64–68.

[67]Peters, D. A. and He, C., "Technical Note: Modification of Mass-Flow parameter to Allow Smooth Transition Between Helicopter and Windmill States," *Journal of the American Helicopter Society*, 2006, pp. 275–278.

[68]Leishman, G. J., *Principles of Helicopter Aerodynamics*, Cambridge University Press, Cambridge, UK, 2000.

[69]AviationToday, *Ask Ray Prouty: Gross Weights Effect on Autorotation*, Danbury CT ., U.S.A., 2007.

[70]Carlson, E. B., *Optimal Tiltrotor Aircraft Operations During Power Failure*, Ph.D. thesis, University of Minnesota, 1999.

[71]Aponso, B. L., Bachelder, E. N., and Lee, D., "Automated Autorotation for Unmanned Rotorcraft Recovery," *AHS International Specialists' Meeting On Unmanned Rotorcraft*, 2005.

[72]Fletcher, T. M. and Brown, R. E., "Main Rotor - Tail Rotor Wake Interaction and its Implications for Helicopter Directional Control," *32nd European Rotorcraft Forum*, 2006.

[73]Fletcher, T. M. and Brown, R. E., "Main rotor - tail rotor interaction and its implications for helicopter directional control," *Journal of the American Helicopter Society*, Vol. 53, No. 2, 2008, pp. 125–138.

[74]Bailey, F. J., "A Simplified Theoretical Method of Determining the Characteristics of a Lifting Rotor in Forward Flight," Tech. Rep. RNo. 716, NACA, 1941.

[75]ART, *FLIGHTLAB Theory Manual (Vol. One & Two)*, Advanced Rotorcraft Technology, Inc., Mountain View CA, 2006.

[76]Voorsluijs, G. M., "A Modular Generic Helicopter Model," Tech. rep., Master Thesis, Delft University of Technology, 2002.

[77]Talbot, P. D., Tinling, B. E., Decker, W. A., and Chen, R. T. N., "A Mathematical Model of a Single Main Rotor Helicopter for Piloted Simulation," Tech. Rep. NTM 84281, NASA Ames Research Center, 1982.

[78]Jewel, J. W. and Heyson, H. H., "Charts of Induced Velocities Near a Lifting Rotor," Tech. Rep. 4-15-59LY, NASA, 1959.

[79]Pavel, M. D., *On the Necessary Degrees of Freedom for Helicopter and Wind Turbine Low-Frequency Mode-Modelling*, Ph.D. thesis, Delft University of Technology, 2001.

[80]Baskin, V. E., Vildgrube, L. S., Vozhdayev, Y. S., and Maykapar, C. I., "Theory of the Lifting Airscrew," Tech. Rep. TT-F-823, NASA, 1976.

[81]Zhao, X. and Curtiss, H. C., "A Study of helicopter Stability and Control Including Blade Dynamics," Tech. Rep. TR 1823T, NASA Ames Research Center, 1988.

[82]Takahashi, M. D., "A Flight-Dynamic Helicopter Mathematical Model with a Single Flap-Lag-Torsion Main Rotor," Tech. Rep. TM 102267, NASA Ames Research Center, 1990.

[83]Murray-Smith, R. and (Ed.), T. J., *Multiple Model Approaches to Modelling and Control*, CRC Press, 1997.

[84]Shamma, J. S. and Athans, M., "Analysis of Gain Scheduled Control for Nonlinear Plants," *IEEE Transactions on Automatic Control*, Vol. 35, No. 8, 1990, pp. 898907.

[85]Shamma, J. and Athans, M., "Gain Scheduling: Potential Hazards and Possible Remedies," *IEEE Control Systems Magazine*, Vol. 12, 1992, pp. 101–107.

[86]Ljung, L., *System Identification: Theory for the User - 2nd Edition*, Prentice Hall, Upper Saddle River, N.J., 1999.

[87]Friedman, J. H., "Multivariable Adaptive Regression Splines," *Annals of Statistics*, Vol. 19, 1991, pp. 1–141.

[88]Klein, V. and Morelli, E. A., *Aircraft System Identification: Theory And Practice*, AIAA Progress in Astronautics and Aeronautics Series, Virginia, 2006.

[89]Tischler, M. B., "System Identification Requirements for High Bandwidth Rotorcraft Flight Control System Design," *AGARD LS-178 Rotorcraft System Identification*, 1991.

[90]Tischler, M. B., "Identification of Bearingless Main Rotor Dynamic Characteristics from Frequency-Response Wind-Tunnel Test Data," *Journal of the American Helicopter Society*, 1999.

[91]Pintelon, R. and Schoukens, J., *System Identification - A Frequency Domain Approach*, IEEE Press, New York, 2001.

[92]Tischler, M. B. and Remple, R., *Aircraft and Rotorcraft System Identification*, American Institute of Aeronautics & Astronautics (AIAA), Reston VA, 2006.

[93]Soderstrom, T. and Stoica, P., *System Identification*, Prentice Hall, 1994.

[94]Chen, R. T. N., "Flap-Lag Equations of Motion of Rigid, Articulated Rotor Blades with Three Hinge Sequences," Tech. Rep. NTM 100023, NASA Ames Research Center, 1987.

[95]Peters, D. A. and He, C. J., "Finite State Induced Flow Models Part II: Three-Dimensional Rotor Disk," *AIAA Journal of Aircraft*, Vol. 32, No. 2, 1995, pp. 323–333.

[96]Gill, P. E., Murray, W., and Saunders, M. A., "SNOPT: An SQP Algorithm for Large-Scale Constrained Optimization," *SIAM Reviews*, Vol. 47, 2002, pp. 99–131.

[97]Gill, P. E., Murray, W., Saunders, M. A., and Wright, M. H., "Users Guide for SNOPT Version 7: Software for Large-Scale Nonlinear Programming," Tech. rep., University of California San Diego, 2008.

[98]SBS-Inc., http://www.sbsi-sol-optimize.com/asp/sol_product_snopt.htm, Stanford University, U.S.A.

[99]Bjorck, A., *Numerical Methods For Least Squares Problems*, SIAM, Philadelphia PA, 1996.

[100]Jategaonkar, R., *Flight Vehicle System Identification: A Time Domain Methodology*, AIAA Progress in Astronautics and Aeronautics Series, Virginia, 2006.

[101]Achar, N. S. and Gaonkar, G. H., "Helicopter Trim Analysis by Shooting and Finite Element Methods with Optimally Damped Newton Iterations," *AIAA Journal*, Vol. 31, No. 2, 1993.

[102]Draper, N. R. and Smith, H., *Applied Regression Analysis*, Wiley, New York, 1995.

[103]Billings, S. A. and Zhu, Q. M., "Model Validation Tests for Multivariable Nonlinear Models Including Neural Networks," *International Journal of Control*, Vol. 62, No. 4, 1995, pp. 749766.

[104]MathWorks, http://www.mathworks.com/, Natick MA., U.S.A.

[105]Peters, D. A., Chouchane, M., and Fulton, M., "Helicopter Trim with Flap-Lag-Torsion and Stall by an Optimized Controller," *AIAA Journal of Guidance*, Vol. 13, No. 5, 1990.

[106]Peters, D. A. and Barwey, D., "A General Theory of Rotorcraft Trim," *Mathematical Problems in Engineering*, Vol. 2, No. 1, 1996, pp. 1–34.